Sensitization of Hypoxic Tumors to Radiation Therapy Using Oxygen Micro-bubbles and Papaverine

by

Haonan Feng

Graduate Program in Medical Physics
Duke Kunshan and Duke University

Date: _____

Approved:

_____
Gregory M. Palmer, Advisor

_____
David Huang

_____
Mark Oldham

Thesis submitted in partial fulfillment of
the requirements for the degree
of Master of Science in the Graduate Program of
Medical Physics in the Graduate School
of Duke Kunshan and Duke University

2020

ABSTRACT

Sensitization of Hypoxic Tumors to Radiation Therapy Using Oxygen Micro-bubbles and Papaverine

by

Haonan Feng

Graduate Program in Medical Physics
Duke Kunshan and Duke University

Date: _____

Approved:

_____
Gregory M. Palmer, Advisor

_____
David Huang

_____
Mark Oldham

An abstract of a thesis submitted in partial
fulfillment of the requirements for the degree
of Master of Science in the Graduate Program of
Medical Physics in the Graduate School
of Duke Kunshan and Duke University

2020

Abstract

Radiation therapy is a frequently used treatment method for malignant tumors despite the heterogeneous response in tumors with a hypoxic microenvironment. Specific features in this microenvironment like poorly formed and inefficient vasculature contribute to chronic and cycling hypoxia. Notably, hypoxic tumor cells are three times more radioresistant than normoxic cells, which make hypoxia a key contributor to poor treatment outcome. There have been many previous attempts to re-oxygenate tumors either through increasing the supply or decreasing the demand of oxygen. However, no study has yet been performed to investigate the combined effect of increasing the oxygen supply and decrease the oxygen demand *in vivo*.

There are two main purposes of this study, which are tested in two individual rounds: 1) assessing the combined effect of oxygen micro-bubbles and papaverine in alleviating tumor hypoxia in murine sarcoma model and 2) assessing the combined effect of oxygen micro bubble and papaverine as radiosensitizers. Using nu-nu mice with subcutaneous sarcoma tumors, the change resulting from oxygen micro-bubbles and/or papaverine was evaluated by changes in hemoglobin saturation from baseline and control groups. By further monitoring tumor growth and percent hemoglobin saturation after administration of papaverine and oxygen micro-bubbles followed by a

single fraction of 15 Gy of radiation, we also tested the effects of the combination of papaverine and oxygen micro-bubbles in tumor control and oxygenation.

The result of the non-irradiated study showed no significant improvement of the combination of oxygen micro-bubbles and papaverine group in the percent hemoglobin saturation level compared with other groups. Notably, percent hemoglobin saturation changes are rather heterogenous within each group. However, this unexpected result may be due to certain practical and theoretic limitations. The follow-up immunohistochemistry study may provide more information of the overall oxygenation of the tumors. For the irradiated study, the percent hemoglobin saturation measurement of the oxygen micro-bubbles and papaverine group is the only one showed improved level the day after the treatment compared with the day before treatment. The combination of oxygen micro-bubbles and papaverine did not show increased tumor control after radiotherapy compared with other groups. However, it should be noted that there are some practical and theoretical limitations in the study that may have contributed in this which is discussed in detail in the discussion chapter. Further studies might be needed to investigate the reasons for this unexpected result.

Contents

Abstract iv

List of Tables viii

List of Figures ix

Acknowledgements xii

1. Introduction 1

1.1 Hypoxia 3

1.2 Hypoxia and Radiation Therapy 5

1.3 Sarcoma 7

1.4 Imaging Hypoxia 8

1.5 Diffuse Optical Spectrometer 11

1.6 Increasing Oxygen Supply (Oxygen Micro-bubbles) 14

1.7 Decreasing the Oxygen Demand (Papaverine) 18

2. Assess the Combined Effect of Oxygen Micro-bubbles and Papaverine in Alleviating Tumor Hypoxia in Irradiated and Non-irradiated Murine Sarcoma Model 20

2.1 Introduction 20

2.2 Material and Methods 23

2.2.1 Tumor Cells 23

2.2.2 Tumor Implantation 23

2.2.3 Overall Workflow 25

2.2.3.1 Non-irradiated Study 25

2.2.3.1 Irradiated Study 30

2.2.4 Papaverine 34
2.2.5 Oxygen Micro-bubbles 34
2.2.6 Quantitative Optical Spectroscopy 36
2.2.7 Radiation Therapy 37
2.3. Results 38
2.3.1 Hemoglobin Saturation for the Non-irradiated Groups 38
2.3.1.1 Oxygen Micro-bubbles Induced Hemoglobin Changes 38
2.3.1.2 PPV Induced Hemoglobin Changes 44
2.3.1.3 Oxygen Micro-bubbles and Papaverine Induced Hemoglobin Changes 46
2.3.2 Radiation Outcome and Oxygenation for the Irradiated Groups 47
2.3.2.1 Radiation Outcome 47
2.3.2.2 Percent Hemoglobin Saturation Changes 52
2.4. Discussion 54
3. Future Work 59
4. Conclusion 61
Appendix A 62
References 66

List of Tables

Table 1: Detailed Procedures for All Four Groups of the Non-irradiated Study 29

Table 2: Detailed Procedures for All Four Groups of the Irradiated Study 33

Table 3: The Dosimetry for Irradiated Study 38

List of Figures

Figure 1: The cartoon illustration of an oxygen micro-bubble with lipid shell, assuming individual units of the shell are wedge-shape 15

Figure 2: A simplified illustration of the relationship of oxygen micro-bubbles, papaverine, and the oxygenation in tumor cells 22

Figure 3: Illustration of tumor volume calculation. The longest diameter is the length, while the vertical one is the width 24

Figure 4: Immobilization device for mice' tail intravenous injection 26

Figure 5: The actual set up for the administration of oxygen micro-bubbles and hemoglobin saturation measurement. 28

Figure 6: The timeline of the non-irradiated study 29

Figure 7: The overall set up in the small animal irradiator 31

Figure 8: The set-up of mice for irradiation 32

Figure 9: The timeline of the irradiated study 33

Figure 10: The changes of hemoglobin saturation in comparison of the baseline with the injection of oxygen micro-bubbles for the OMB group. 39

Figure 11: The changes of hemoglobin saturation in comparison of the baseline with the injection of oxygen micro-bubbles for the OMB&PPV group 41

Figure 12: The changes of hemoglobin saturation in comparison of the baseline with the injection of oxygen micro-bubbles for the OMB&PPV group 43

Figure 13: Individual data points demonstrating the percent hemoglobin saturation before and 29 minutes after the administration of papaverine for the OMB&PPV group. 44

Figure 14: Individual data points demonstrating the percent hemoglobin saturation before and 29 minutes after the administration of papaverine for the PPV group 44

Figure 15: Individual data points demonstrating the percent hemoglobin saturation before and 29 minutes after the administration of papaverine for the vehicle group 45

Figure 16: The percent hemoglobin saturation changes with administration of oxygen microbubbles, papaverine and or equivalent amount of saline 46

Figure 17: The survival curve for the irradiated study 47

Figure 18: The survival curve with the endpoint of five times the original tumor volume 48

Figure 19: The number of censored mice and the ones that reached endpoint for all four groups in the irradiated study 49

Figure 20: The graph demonstrating the tumor growth include all mice of the irradiated study 50

Figure 21: The graph demonstrating the tumor growth include all mice of the irradiated study excluding the censored mice 50

Figure 22: The graph demonstrating the tumor growth include all mice (excluding censored mice) of the irradiated study normalized to day one 51

Figure 23: The graph demonstrating the percent hemoglobin saturation changes include all mice of the irradiated study 52

Figure 24: The graph demonstrating the percent hemoglobin saturation changes for all mice of the irradiated study normalized to the day before the treatment 52

Figure 25: Tumor growth for all mice from the PPV+RT group 62

Figure 26: Tumor growth for all mice from the OMB +RT group 62

Figure 27: The tumor growth for all Mice from OMB&PPV+RT group 63

Figure 28: The tumor growth for all mice from RT Only group 63

Figure 29: The percent hemoglobin saturation for all mice from the PPV+RT group 64

Figure 30: The percent hemoglobin saturation for all mice from the OMB+RT group 64

Figure 31: The percent hemoglobin saturation for all mice from the OMB&PPV+RT group 65

Figure 32: The percent hemoglobin saturation for all Mice from the RT Only group 65

Acknowledgements

I would like to express my greatest gratitude for my advisor, Dr. Gregory Palmer in the Department of Radiation Oncology at Duke University, for everything he has done in the past year. Dr. Palmer has been nothing but supportive and extremely helpful, everything a student could ask for from an advisor. I am grateful for his guidance throughout the experiment and thesis drafting. I really appreciate his patience and encouragement during the entire journey, I could never come this far without his help. Thank you so very much for always being there for my numerous questions.

I also would like to thank the other two committee numbers, Dr. Mark Oldham in the Department of Radiation Oncology Physics in Duke University and Dr. David Huang from Duke Kunshan University for their supports. Dr. David Huang has shared his invaluable knowledge and life wisdom with me many times when I stuck in reverse.

I would also like to thank everyone in Dr. Palmer's lab for their generous help. I would like to thank Ashlyn Rickard for her enormous help on this project. I am grateful that she pointed me into the direction when I had no clue how things worked in a lab, and all the long hours she spent with me for the experiment. Many thanks to Antoine Mansourati, who was kind enough to help me with the monitoring of those mice. Many thanks also to Kenneth Young, for teaching me how to use all those machines in the lab and sharing his knowledge about Immunohistochemical staining. Thanks to Dianne Young, who helped so much with all the paperwork.

I would also like to acknowledge Dr. Virginie Papadopoulou in the Department of Biomedical Engineering at the University of North Carolina at Chapel Hill and Dr. Traci Reusser in the Department of Mechanical Engineering at the University of Colorado. Dr. Recusser has been much helpful providing the oxygen micro-bubbles needed for the treatment. Dr. Papadopoulou was responsible for all the administrations of oxygen micro-bubbles. Apart from that, Dr. Papadopoulou was most kind to show us Dr. Borden's lab and let us sit one of their own oxygen micro-bubbles treatment.

I am also obliged to the faculty at Duke Kunshan University for their help and extra efforts under this special circumstance. Thanks to Dr. James Bowsher's many emails about the timeline about the thesis defense and courses, such that working at home was a possible option. Thanks to Claire Luo, who kept us updated with everything academically and more. Thanks also to all the staff who were still doing everything they can helping everything running smoothly during this changing time.

I would also like to thank my family for always believing in me and always being there. I am so grateful for everything you have done for me for the last twenty-four years.

A final thanks to everyone fighting in the front line against the COVID-19 worldwide. Thank you all so much for your efforts and dedications.

1. Introduction

Solid tumors often contain hypoxic regions owing to certain characteristics like poorly-formed, leaky vasculature.[1] Hypoxia are generated due to the fact that the oxygen supply is not sufficient for the oxygen demand of the cancerous tissues.[2] Tumor hypoxia has a negative impact for all types of treatment, including surgery, radiotherapy (RT), immunotherapy, transplants, and chemotherapy.[3 - 5] It has long been known to be a significant obstacle for satisfactory radiation treatment outcomes[6] owing to its effect in increasing radiation resistance in hypoxic cancerous cells by as much as three times compared with normoxic cells.[3] Since more than half of cancer is be treated with radiotherapy,[7] tumor hypoxia is of great concern clinically. Hypoxia can be divided into two types depending on the duration of low partial pressure of oxygen (pO_2) in the microenvironment. The hypoxia is chronic when the microenvironment sustains low pO_2 status and is considered as cycling when the pO_2 level fluctuates periodically. Theoretically, an increase in tumor oxygenation could be achieved by two approaches: increasing the oxygen supply or decreasing the demand of oxygen in tumors. Current methods designed for these purposes include hyperbaric oxygenation,[8] inhaled carbogen,[9] nitroimidazole,[10] oxidative phosphorylation,[11] and mitochondria respiration inhibitors.[57]

However, most of them are limited by vasoconstriction, practical administration, biological half-life and normal tissue toxicity.[8 -11] Recently, oxygen micro-

bubbles have made several advances by offering an acute increase in tumor oxygen supply.[12] Compared with previous attempts to increase oxygen supply in general, oxygen micro-bubbles provides oxygen in a more localized manner. Papaverine, an FDA-approved drug as a smooth muscle relaxant has also been identified as a radiosensitizer for radiation therapy by inhibiting mitochondrial metabolism.[13] As a vasodilator, papaverine can prevent vasoconstriction. However, there are no experiments that study the combined effect of oxygen micro-bubbles (increase the oxygen supply) and papaverine (decrease the oxygen demand) *in vivo*, which may offer a higher potential for radiosensitizing solid tumors. Due to their potentials in alleviating hypoxia the cancerous tissues, The Palmer Lab at Duke University, in collaboration with the Dayton Laboratory at University of North Carolina at Chapel Hill, has pioneered in testing the combing effect of oxygen micro-bubbles and papaverine in radiosensitizing flank sarcoma tumors in murine models. Previous studies have shown that 1) oxygen micro-bubbles significantly increase dissolved oxygen content *in vitro*,[15] and when inject intratumorally into rat fibrosarcoma model;[46] 2) papaverine has been proven to radiosensitize tumors in mouse E0771 and A549 models.[13] The purposes of this study are to 1) assess the combined effect of oxygen micro-bubbles and papaverine in alleviating tumor hypoxia in murine sarcoma model. We hypothesize that oxygen micro-bubbles and papaverine will improve tumor oxygenation and that the combined effect of oxygen micro-bubbles and papaverine will improve tumor oxygenation more than either

oxygen micro-bubbles or papaverine alone; 2) assess the combined effect of oxygen micro bubble and papaverine as radiosensitizer in murine sarcoma model. We hypothesize that oxygen micro-bubbles and papaverine prior to radiotherapy can increase the therapeutic effect of radiation treatment more than the injection of either oxygen micro-bubbles alone with radiotherapy, papaverine alone with radiotherapy or radiotherapy alone.

This chapter will discuss some key concepts relevant to this work in further detail. Chapter 2 will cover the experimental details and results of assessing combined effect of oxygen micro-bubble and papaverine in alleviating tumor hypoxia in non-irradiated models and its effect as radiosensitizer in irradiated murine sarcoma models. Then the following chapter will be the discussion of the entire work. A chapter of potential interesting further investigations and another chapter of conclusion will also be included.

1.1 Hypoxia

A common characteristic of solid tumors,[1] hypoxia plays a critical role in radio resistance and has been associated with poor clinical outcomes. Defined as a deficiency in the partial pressure in the tissue, hypoxia is defined by tissue partial pressure that falls below 10 mm Hg.[14] Tumors are commonly hypoxic compared with the surrounding healthy tissues due to the fact that the oxygen supply is insufficient for the oxygen demand in the microenvironment of tumors. There are numerous mechanisms for the

formations of tumor hypoxia. From the perspective of physiology, tumor hypoxia is formed because of : 1) relative sparse arteriolar supply; 2) inefficient network of vasculatures ; 3) low-density vascular, which could not meet the requirement of diffusion distance limitation (70-100μm); 4) fluctuant red blood cell flux in microvessels; 5) inconsistent oxygenation at areas nearer the arteriolar network and those further away; 6) hypoxic red blood cells; 7) divert blood flow shunted;[15] 8) cyclical hypoxia.[15.]

Hypoxia arises via different mechanisms and is often divided into two categories depending on the persistence of low pO_2 conditions. One is chronic hypoxia, the other one is cyclical hypoxia. The chronic hypoxia arises in areas whose partial pressure in the blood is less 10 mm Hg for a long period of time, while the cyclical hypoxia is referring to tissues that undergo dynamic changes of pO_2 which can vary 20 mm Hg (in murine squamous model based on measurements from electron paramagnetic resonance imaging in a time widow of 30 minutes).[16, 67] The cause of the cycling hypoxia is believed to be the instabilities in red cell flux in the microvascular of tumors and temporary fluctuations of perfusion. The frequency of cycling hypoxia can be as fast as 2 to 3 cycles per hour.[17] However, even similar changes of perfusion would result in different overall oxygenation for different regions of the tumor. The main consequences of tumor cycling hypoxia are: 1) a more sensitive response of hypoxia inducible transcription factor 1 (HIF-1) compared with chronic hypoxia; 2) an increased level of free radicals;[18]

When the tissue become hypoxic, cells produce more genes that are regulated by HIF-1, which has been called "master regulator of oxygen homeostasis".[19] HIF-1 is produced continuously in the cells; however, the activity of HIF-1 decreases when there is oxygen present. HIF-1 stabilizes and binds to key genes in the nucleus when the oxygen level falls, and therefore causes transcription of those genes. Genes that are usually involved in this process are: 1) genes that are involved in angiogenesis, for example, vascular endothelial growth factor (VEGF);[69] 2) genes that are related to the anaerobic glycolysis, for example, glucose transporter 1 (GLUT1);[70] and 3) genes that regulate PH level, for example, carbonic anhydrase 9 (CA9).[70] Among those transcriptions, VEGF is the gene that stimulates vasculature formation in tumor. The blood vessels in tumors are usually leakier and poorly functional compared with vessels that are developed under the normal cellular homeostatic microenvironment, causing some tumor cells to become acutely hypoxic and those distant from blood vessels to be chronically hypoxic. These characteristics of tumor vasculature also allows metastasis to occur since the tumor cells can penetrate into the circulatory system through those leaky vessels.

1.2 Hypoxia and Radiation Therapy

Though chronic and cycling hypoxia affect tumor growth in different ways, they both result in radio resistance. For photons to obtain their tumor-killing effects, they have to interact with cancerous or noncancerous tissue (photons may interact with

noncancerous tissue and produce secondary electrons that distribute energy into cancerous tissue directly or through free radicals) and release their energy into the tumor cells to cause a DNA strand break. There are two ways that radiation interacts with tissue: one is excitation, which causes elections within atoms to move up to a higher-energy orbital or excites the atoms or molecules; another one is ionization, which occurs when the electron gain enough energy to be free from the atom or molecule and become secondary electron. DNA is the target for radiotherapy for direct or indirect damages. Direct damage to the DNA is through direct interaction between the secondary electrons. Indirect action is created by those unpaired electrons, producing free radicals (made of unpaired electrons and part of the molecule) that are able to diffuse far enough to break single DNA strands. Among various free radicals, hydroxyl (.OH) radical is the most prevalent one, and it is created through ionizing water which makes up most of the human body. Indirect damage to DNA is caused mainly by hydroxyl. However, in the presence of molecular oxygen, another radical: peroxyl radical is created, which can stabilize more irreparable damage to the DNA,[20] and increase radiation toxicity by two and half fold.[21]

At low oxygen concentration, the percentage of cycling cells is also low and drug efficacy might be compromised because of that. Apart from that, the activation of hypoxia inducible factor-1 (HIF-1) is also of great importance for radio resistance, which also is affected by the oxygenation level. Therefore, the absence of oxygen may also

cause a decreased number of DNA double-strand breaks, which is the type of DNA damage that is more difficult to repair.

Many studies have shown that the undesirable outcome after radiation treatments is closely related to hypoxia in solid tumors.[22-24] Results of these studies show that tumor hypoxia is correlated strongly with radioresistance. Reoxygenation is therefore of great importance for improving the radiation treatment outcome. It is also one the reasons fractionation schemes would work better than single fraction schemes since they allow the cancer cells to reoxygenate between treatment fractions.

1.3 Sarcoma

The long-term goal of this pilot study is to contribute to a 5-year project that is aimed for testing the effectiveness on larger animals before use in clinical trials. Due to factors like species-specific differences in drug metabolism, tumor burden, and immunocompetence, the correlation between murine studies and clinical trials are extremely poor.[68] Dogs are ideal translational models owing to their relatively larger sizes, immune status similar to humans and outbreeding. Since soft tissue sarcoma comprises 15% of skin and subcutaneous cancers in the dogs,[25] and it resembles soft tissue sarcoma in humankind, therefore it is chosen as the experimental tumor model. Apart from that, sarcoma is also preferred for its peripheral orthotopic location, which makes it feasible for serial imaging and biopsy.[26] Besides, spontaneous sarcoma will commonly naturally develop therapeutic resistance as well as spontaneous metastasis.

1.4 Imaging Hypoxia

Numerous studies have shown the significant role hypoxia plays in metastasis,[27] chemoresistance,[28] and radio resistance.[29] Thus, knowing the extent and degree of hypoxia in a tumor prior to the treatment is of great importance. Based on the features of hypoxia,[15] there are certain requirements the imaging system has to meet: 1) being able to distinguish hypoxia, normoxia and necrosis; 2) sensitive to the oxygen partial pressure at clinically relevant level (0 to 10 mmHg); 3) being able to identify cellular oxygen partial pressure opposed to vascular ones; 4) have good spatial resolution which can distinguish 80 to 100 μm for the oxygen level can change steeply within several micrometers; 5) have the ability to obtain images 2 to 3 times within an hour, based on the fastest frequency of red cell flux, which is the depending factor of cyclical hypoxia; 6) not restricted by the depth of tumor; 7) noninvasive and repeatable; 8) ease of use.[30]

A variety of techniques are being proposed for the purpose of quantifying tumor hypoxia. There are mainly two ways for them to obtain oxygen information: 1) direct measurement, the imaging systems that fall in this category include blood oxygen level dependent magnetic resonance imaging (BOLD-MRI) and near-infrared spectroscopy (NIRS); 2) indirect measurement through quantifying either exogenous hypoxia markers or endogenous hypoxia markers, the parameters that are connected with the oxygen level in cells.[30]

The polarographic electrode is considered the "gold standard" in oxygen sensing. It generates electric current from cathodes that would decrease when there is oxygen present. The intensity of the current is proportional to the partial pressure of oxygen. However, it has its limitations due to its invasive nature, for example when performing real-time measurement. In addition, it can only measure oxygenation at specific points.

Immunohistochemical staining (IHC) against hypoxia markers is also one of the most frequently used techniques that can provide quantitative information on the oxygenation of tumors. It is based on the specific binding between the antibody and the antigen.[31] First of all, antigens or half-antigens are fabricated though certain chemical substances extracted from the tissue or cells. Then after injecting these antigens into animals, antibodies are manufactured and used for detecting the antigens using immunofluorescence imaging of tissue sections. Hypoxia markers are injected into the living subject before the tumor removal is performed. Several have been developed for this purpose. Among them, EF5 is the most frequently used one. Under the pressure of 10 mm Hg, the nitroimidazole undergoes a nitroreductase-catalyzed single electron reduction. Together with cellular macromolecules, it produces covalent bonds, therefore trapping EF5 inside the hypoxic cells.[32] IHC can provide information of the relationship between the oxygen partial pressure and blood vessel distribution of the tumor. However, even though IHC can provide important information of the

microenvironment of the cancerous tissue, it has its limitations as a terminal technique, and that is when non-invasive hypoxia imaging devices come into play.

Positron Emission Tomography (PET) is one of the commonly used non-invasive imaging devices to image hypoxia. The basic physics of PET is positron-electron annihilation. Take one of the most frequently used radiopharmaceuticals, ^{18}F-fluoromisonidazole (FMISO), as an example. It would bind to intracellular macromolecules and build up in hypoxic cells. Low uptake would indicate high tissue oxygen concertation for the uptake is proportional to the level of hypoxia. As a short-lived position is emitted by ^{18}F, it will have an annihilation interaction with a nearby electron and produces two 0.511 Mev photons and those two photons would go into opposite directions. By detecting those two 0.511 Mev photons at the same time by the usage of ring detectors, we would be able to tell the site of the interaction though filtered back projection algorithm. However, despite its unique advantage in providing physiologic information, PET images usually do not have enough information about the anatomy, which can be fixed by combing it with computed tomography (CT).However, this imaging is still very time consuming.

Another commonly used non-invasive imaging device is magnetic resonance imaging (MRI). MRI provides a spatial map in which each voxel represents the micromagnetic properties of the tissue corresponding to that point. In MRI, the patient is placed into a magnetic field, radio waves will be generated by coils and their energy will

be absorbed by the protons in human body. Subsequently, the absorbed energy will be reemitted from the protons once the radio wave is removed and the time is dependent on the magnetic properties of the tissue. Blood oxygenation level-dependent (BOLD) MRI is also a commonly used hypoxia imaging that uses deoxyhemoglobin as contrast. More deoxyhemoglobin corresponding to more magnetic susceptibility, which indicate shorter T2* which accounts for spin-spin relaxation. Therefore, lower MRI signal intensity in BOLD MRI images would indicate more deoxyhemoglobin. However, MR is also limited by various artifacts.

Electron paramagnetic resonance oximetry (EPR) imaging is another hypoxia imaging device that is able to offers a 3D oxygen map that directly quantifies pO_2 of the cancerous tissue. The physics of EPR are similar to MRI, only instead of detecting proton spin dephasing, EPR is using electron spin dephasing.

Optical imaging techniques are also frequently used for hypoxia imaging for its advantages in real time imaging for point measurements in preclinical studies.

1.5 Diffuse Optical Spectrometer

The most commonly used principle of optical hypoxic imaging is based on the differences of oxygenated and deoxygenated hemoglobin in the tissue absorption spectra,[33] and they can be used for the calculation of hemoglobin oxygen saturation. Diffuse optical spectroscopy, photoacoustic tomography and optical coherence tomography all fall into this category.

The diffuse optical spectroscopy system consists of a light source and UV-NIR (ultraviolet-near-infrared) spectrometer that quantifies aspects of chemoresponses in turbid media.[34] The light source emits light with wavelength from 300 to 900 nanometers, in the range of interest of soft tissue, and analyzes the reflected signal spectrum which is quantified using the spectrometer. Unlike conventional optical physics, which is based mainly on the fact that the pathways of the rays of light are almost straight, photons in diffuse optical spectrometer will take a random path through the media and hence "diffuse" in the media. In this case the actual path of the photons is a statistical probability. Therefore, spatial resolution is sacrificed in order to improve the penetration depth. Oxyhemoglobin and deoxyhemoglobin are the most important dynamic chromophores in the range of UV-NIR. The quantitative optical spectroscopy can obtain the reluctance spectra. The changes of oxyhemoglobin and deoxyhemoglobin are proportional to changes of the light detected in transillumination. The relationship between the optical density and light intensity is governed by the Beer-Lambert law, which is shown in Equation [1.1].

$$OD = -\log\frac{I}{I_0} \qquad [1.1]$$

OD stands for optical density, I is the transmitted light intensity, I_0 is the original light intensity. The concertation of the solution [X] can be worked out from the optical density through Equation [1.2]:

$$OD = \varepsilon \cdot [X] \cdot L \qquad [1.2]$$

L is the length the light has passed through the container. ε is the molar extinction coefficient for the compound, which describes the amount of light to be absorbed. In this case, ε of the hemoglobin differs for oxyhemoglobin and deoxyhemoglobin. Theoretically, the extinction coefficient also varies with temperature, PH, and osmolality.[35] However, these factors are neglected since they usually change very little during the measurement. [35] The media can be modeled as a mixture of various constituents. The absorption coefficient of the media is a proportional to the contribution from each ingredient:

$$\mu_{A=\Sigma_i \varepsilon_i \cdot ln10 \cdot [X_I]} \qquad [1.3]$$

Quantitative optical spectroscopy can obtain the reflected spectra through the probe. Then with the distribution of path length generated using the Monte Carlo model the absorption coefficient of the tissue could be found. Quantitative optical spectroscopy offers various benefits, which include: 1) the measurement takes less than 1 second and the result is gained immediately; 2) harmless, non-invasive measurement over time for small animal; 3) quantitative analysis.

Optical spectroscopy can measure both oxygenated hemoglobin (HbO_2) and deoxygenated hemoglobin (dHb). Total blood concentration (THb) and the percent oxygenation saturation (SO_2) can be also obtained through:

$$\mathrm{THb} = \mathrm{HbO_2} + \mathrm{dHb} \qquad [1.4]$$

$$\mathrm{SO_2} = 100 \times \frac{\mathrm{HbO_2}}{\mathrm{THb}} \qquad [1.5]$$

Therefore, diffuse optical spectroscopy is preferred for its ability as a non-invasive device to quantify hemoglobin saturation and act as a marker for vascular oxygenation.[40-42]

1.6 Increasing Oxygen Supply (Oxygen Micro-bubbles)

As one of the significant factors that influences the outcome of radiotherapy treatments, reoxygenation has been of interest for decades. Intuitively, one would consider providing hypoxic cancerous tissue with extra oxygen through increasing the oxygen supply, and methods have been raised and tested preclinically and clinically.[8-10] For example, hyperbaric oxygenation,[8] inhaled carbogen,[9] and nitroimidazole[10] are proposed for this purpose. Hyperbaric oxygenation is a therapy that exposes patients under a high, breathable oxygen environment with hyperbaric pressure in order to saturate blood with oxygen. This is widely used for decompression sickness in the clinic. Carbogen is the mixture of 95% of oxygen and 5% of carbon dioxide which has also been extensively tested. Theoretically, with the presence of carbon dioxide in the mixture, vessels would be more dilated than with pure oxygen, and it will increase cardiac output through positive chronotropic effects and shift the oxygen-hemoglobin dissociation curve, according to Kruuv *et al.* [63] The proportion of carbon dioxide is set for optimal effort of carbon dioxide while not causing physiological discomforts to patients. However, it has been shown that the carbogen dioxide may be counterproductive in certain situations.[9] Other methods mentioned above are also limited by normal tissue toxicity, vasoconstriction and practical administration difficulties. In order to relieve

tumor hypoxia during radiotherapy through providing additional oxygen, another technique has been proposed recently.

Micro/nano-bubbles have been used as contrast for ultrasound and photoacoustic imaging for decades and have showed their potential as solutions for the conundrum owing to certain characteristics: 1) lager surface contact area; 2) higher payload: 3) higher cellular uptake; 4) smaller size; 5) polydisperse size distribution; 6) efficient gas delivery. Micro/nano-bubbles (MNBs) are named owing to their sizes. MNBs are spherical shaped vesicles that are composed of shell and core. The core is usually filled with medical gases, while the shell is made of biocompatible materials. For example, an oxygen loaded microbubble with lipid-based shell has been depicted below in Figure 1.

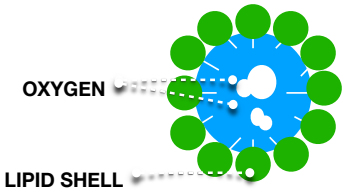

Figure 1: The cartoon illustration of an oxygen micro-bubble with lipid shell, assuming individual units of the shell are wedge-shape

There are three important factors that need to be optimized in order for the MNBs to pass though the blood capillaries: 1) size: 2) stability 3) surface coating; therefore, the most frequently used size range of MNBs is from 0.1 to 20 μm, even though a larger size

would provide better echogenic owing to higher backscatter of ultrasound. The stability of MNBs is correlated with pressure differences between the interior and exterior of core, the Laplace pressure.[71] These differences are given by the formula [1.6] as follows:

$$\Delta P = Pin - Pout = \frac{2\delta}{r} \qquad [1.6]$$

In which δ stands for the interfacial tension while *r* accounts for the radius of the bubble. As the equation indicates, in order to gain a good stability or decrease the Laplace pressure, there are two approaches. One is increasing the radius of the bubble, the other is decreasing the interfacial tension via surfactants.[71]

The bubbles would dissolve within seconds without shells due to the high solubility of oxygen, and direct injection of oxygen would cause hemolysis. There are several types of shells that are dedicated for different purposes. First of all, a lipid-based shell is the most preferred kind for medical applications owing to its biodegradability and biocompatibility. Its stiffness is governed by the length of hydrocarbon chains. The longer the chains, the more cohesive the bubbles. Various combinations of base phosphides have been used in combination with numerous surfactants and emulsifiers. Polyethylene glycol (PEG) is commonly used for improving stability and circulation time, because it is non-toxic and highly hydrophilic. Apart from stabilizing, PEG can also 1) reduce immunogenic responses; 2) decrease plasma clearance; 3) increase half-life; 4) prolong circulation.[36-39]

Apart from being biocompatible, protein-based shells are also stable, amphipathic, biodegradable and long-lasting. Protein-based shells are produced through heating the protein solutions and emulsifying them. Protein shells have a lower diffusion coefficient compared with lipid shells owing to the disulfide bonds between the thiol groups of cysteine.[71]

Polymer shells are usually larger than lipid shells and protein shells, which enable higher drug-loading capacity. However, they are also more resistant to ultrasound fields, and require higher pressure applied for oscillations.

There are two ways for the MNBs to deliver oxygen once they are injected into the circulation system. One of them is by applying pressure through high-intensity ultrasound. The pressures generated would resonate and rupture the MNBs and thereby release the gases in them. The other method is the spontaneous approach, for the shell radius would decreases as the core gases leaking and cause the Laplace pressure to increase, thereby breaking the bubbles at some point. The bubbles will break completely under this circumstance after a period of time. However, for the bubbles to break and deliver their contents to a specific location, the first approach is preferred. The transformation of MNBs is dependent on the amplitude of ultrasound. First of all, the volume of the bubble is inversely correlated with the pressure differences caused by ultrasound at low acoustic power when the mechanical index is lower than ten percent. Secondly, for modest acoustic power with mechanical index ranges from ten to thirty

percent, the bubbles become more resistant and develop a non-linear oscillation. Then as the acoustic power continues to increase to the range of thirty to sixty percent of the mechanical index, the bubbles will undergo forced expansion and compression. The gases inside would diffuse either through the large shell defects or though the complete fragmentation of the shell.

1.7 Decreasing the Oxygen Demand (Papaverine)

An alternative way to alleviate hypoxia in cancerous tissue is to decrease tumor-cell oxygen consumption. Potentially, this approach would have some advantages compared with increasing the supply owing to the nature of the poorly formed vessels in the cancerous tissue for they would be a barrier for oxygen transportation and distribution. Oxygen is a key factor of aerobic respiration, which is the process that breakdown glucose and release energy, adenosine triphosphate (ATP). As the largest complex of the mitochondrial electron transport chain, Complex I (NADH-ubiquinone oxidoreductase) contributes greatly to the membrane that support ATP synthesis.[51] Complex I is responsible for providing electron acceptors and regenerating oxidized cofactors which are helpful in sustaining proliferation of cells.[52,53] In addition, Complex I is also maintaining the NAD^+/NADH ratio which 1) is a necessary factor for the activity of mitochondrial malate dehydrogenase;[52,53] 2) generates aspartate;[52,53] 3) stabilizes hypoxia-inducible factor-1-alpha (HIF 1α).[54] Complex I inhibitors cause an imbalance between NAD^+ and NADH, give rise to extra NADH. This accumulation results in

tumor growth arrest through complex enzyme changes.[54-56] Interestingly, Li *et al*. have also demonstrated that Complex I may have negative impact on the mitochondrial permeability transition pore which is responsible for apoptosis and necrosis.[61] Therefore, an inhibitor of Complex I may result in apoptosis. Another approach, alleviating hypoxia through decreasing the demand of oxygen in tumor has been proposed and tested. However, these applications have been limited by their biological uptake, half-life, and toxicity *in vivo*.[57] Recently, Martin B. *et al.* had proposed an FDA-approved drug-- papaverine, a commonly used vasodilator, as a solution.[13] Papaverine is used to treat disorders of stomach or gallbladder, chest pain, circulation problem, heart attack and vasospasm smooth muscles. Martin B. *et al.* had conducted genetic analysis that showed papaverine's ability as an inhibitor for Complex I. Additionally, their work showed that for mice injected with papaverine, there was a significant increase in partial oxygen pressure within the first 30 to 45 minutes.[13] Mice were irradiated 30 minutes after the papaverine treatments, resulting in two to fourfold more effective tumor control than the group only received radiotherapy.[13] An increased therapeutic index and a modest radioprotective effect of papaverine treatment was also observed in the E0711 tumor model through jejunum analysis of H&E and Ki67 stained sections.[13]

2. Assess the Combined Effect of Oxygen Micro-bubbles and Papaverine in Alleviating Tumor Hypoxia in Irradiated and Non-irradiated Murine Sarcoma Model

2.1 Introduction

Characterized by topspeed cell proliferation, tumors generally develop sparse and poorly formed vasculature that does not provide adequate oxygen supply to the cancerous tissues, leading to tumor hypoxia. Several studies conducted have showed its negative impacts on surgery, chemotherapy and radiation therapy.[3-5] Höckel *et al.*, Nordsmark *et al.*, and Brizel *et al.* have all shown that hypoxia can influence the treatment outcome and overall patient survival. Due to its effect on oxygen-dependent free radicals and hypoxia-inducible transcription factor-1 complex signaling, hypoxia is a key factor that impacts radiation treatment outcomes. Theoretically, an acute increase in tumor oxygenation could improve the radiotherapy outcome. Several techniques have been proposed for this purpose.[8-10] The mixture of oxygen and carbon dioxide had been studied as a radiosensitizer for it is believed that CO_2 could alleviate vasoconstriction caused by O_2 and have potential to increase blood flow in certain tissue. While Rojas *et al*. showed carbogen's effect in improving radiation treatment,[43] Dewhirst *et al.* showed the opposite.[44] Nitroimidazoles have also been proposed for improving radiotherapy index through hypoxic modification.[45] However, Breider *et al*. showed that it would induce toxicity when tested in cynomolgus monkeys.[46]

Instead of raising the overall oxygen, another approach is to increase the oxygen supply in specific location. Recently, Borden *et al*. has made some progress with lipid-based oxygen micro-bubbles.[12] Borden *et al.* showed an increase in percent hemoglobin saturation in asphyxiated animals when injected oxygen micro-bubbles intratumorally.[48,49] Oxygen micro-bubbles deliver acoustically activated oxygen as its core gases, which are triggered to burst in a specific location by ultrasound. Apart from being safe, inexpensive and portable, ultrasound can also be used for imaging the target in real time. Progress has also been made through an alternative way of increasing oxygen supply. Benej *et al.* proposed papaverine, an FDA-approved smooth muscle relaxant, as a radiosensitizer. It has shown great potential for improving RT tumor control by inhibiting mitochondrial metabolism.[13] Intuitively, the combination of oxygen micro-bubbles and papaverine would increase tumor oxygenation both by increasing oxygen supply and decreasing oxygen demand, as shown in Figure 2. In addition, Secomb *et al.* conducted a simulation of the combination effect of reduced oxygen consumption and hyperoxic gas breathing and confirmed the existence of the synergistic effect which indicate greater potential of the combination of micro-bubbles and papaverine.[64] The Palmer Lab at Duke University, in collaboration with the Dayton Lab at University of North Carolina at Chapel Hill, has pioneered a study to test the combination effect of oxygen micro-bubbles and papaverine in radiosensitizing flank sarcoma tumors in murine models. Initially developed as a contrast agent for

ultrasound, micro-bubbles are also used for drug delivery. Dr. Dayton's Lab at University of North Carolina at Chapel Hill developed oxygen micro-bubbles with longer acyl-chain phospholipids, which made the shells stiffer, increasing circulation persistence.

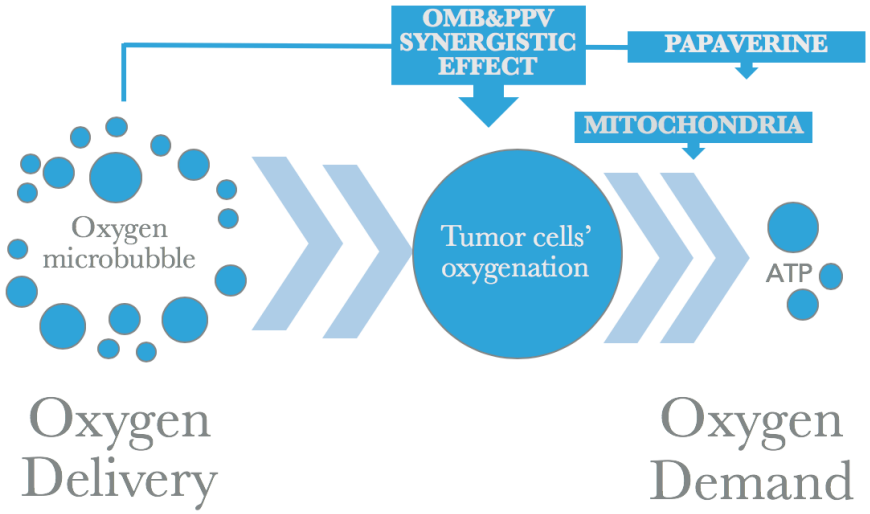

Figure 2: A simplified illustration of the relationship of oxygen micro-bubbles, papaverine, and the oxygenation in tumor cells

There are two main purposes of this study, which are tested in two separate studies. In the first study, the combined effect of oxygen micro-bubbles and papaverine in alleviating tumor hypoxia in murine sarcoma model was assessed. This was conducted on nu-nu mice with KP sarcoma tumors, and they were treated with papaverine and oxygen micro-bubbles. The oxygenation was evaluated through hemoglobin saturation measurement conducted via diffuse optical spectroscopy. In the second study, the combined effect of oxygen micro-bubbles and papaverine was assessed as a radiosensitizer in murine sarcoma model. By monitoring tumor growth

and tumor oxygenation after a single fraction of 15 Gy radiation treatment and administration of papaverine and oxygen micro-bubbles, we also tested the effect of the combination of papaverine and oxygen micro-bubbles in improving radiation treatment outcome.

2.2 Material and Methods

2.2.1 Tumor Cells

Sarcoma (KP cell line) cells used for this experiment were developed in Kirsch Lab of the Department of Radiation Oncology at Duke University. Tumor cells were propagated from a primary sarcoma of a genetically modified mouse model (GEMM). KP Cells were cultured in complete media: Dulbecco Modified Eagle's Medium (DMEM, 10% fetal bovine serum (FBS), L-glu and penicillin-streptomycin (pen/strap) solution. They were spilt at 1:20 about every three to four days. Cells were incubated in a humidified environment of 37C° in a 5 % CO_2, 95% air incubator.

2.2.2 Tumor Implantation

All animals used in this experiment were approved by the Duke University Animal Care and Use Program. All animal experiments preformed were according to protocols approved by Institutional Animal Care and Use Committee (IACUC) and were under regular veterinarian observations.

For the non-irradiated groups, twenty immunocompromised nu/nu female mice (4-6 weeks old, sourced from Duke's Internal Breeding Program) were implanted with

200 000 sarcoma (KP) cells in their right flank. After the implantation, mice were monitored thrice weekly for weight and tumor growth. Humane endpoints of a loss of more than 15% of its original weight or tumors greater than 1500mm^3 were observed. Tumors were measured with calipers, and the volume were calculated using the formula [2.1], which is also illustrated in Figure 3. All length and width measurement were rounded into two decimal places.

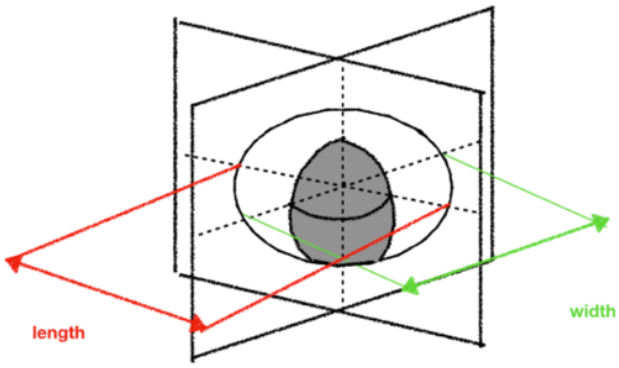

Figure 3: Illustration of tumor volume calculation. The longest diameter is the length, while the vertical one is the width

$$volume = \frac{\pi}{6} \times length \times width \times width \qquad [2.1]$$

Once the tumors have reached volumes of 300-500 mm^3, they were randomized by tumor size into four groups: 1) injected with both oxygen micro-bubbles and papaverine (OMB&PPV); 2) injected only with micro-bubbles (OMB); 3) injected only with papaverine (PPV); 4) vehicle group. All mice had the same time to accumulate

tumors. All mice were identified through implanting numerically coded RFID microchips.

For the second study looking at radiation response, thirty-five immunocompromised nu-nu female mice (6-8 weeks old, sourced from Duke's breeding core) were implanted with 200 000 sarcoma (KP) cells in their right flank. After implantation, mice were monitored as described above. Once the tumors reached volumes of 100-200 mm^3, they were randomized by tumor volume into four groups and been treated with a single fraction of 15 Gy: 1) injected with both oxygen micro-bubbles and papaverine plus radiation treatment (OMB&PPV+RT); 2) injected with only micro-bubbles plus radiation treatment (OMB+RT); 3) injected with only papaverine plus radiation treatment (PPV+RT); 4) only radiation treatment (RT only). The mice were humanely sacrificed according to our approved protocol either at the time of endpoint measurement or when the maximum tumor burden of 1500mm^3 was reached.

2.2.3 Overall Workflow

2.2.3.1 Non-irradiated Study

All experiments were performed under room temperature, heating pad were used for mice' body temperature maintenance. All mice of the same group were treated on the same day. All mice were treated in two days continuously.

The mouse was first measured for its hemoglobin saturation (Hb sat) through the usage of Zenascope optical spectrometer (Zenalux, Durham, NC, USA) before all

treatments to quantify the original oxygenation of the tumor (T= -1minute). Then mice were put into a specific immobilization device (Braintree scientific Inc., MA, USA), as shown in Figure 4, for the tail intravenous injection of papaverine (5 mg/Kg or vehicle) (T=0). For mice that were from other groups, OMB group and vehicle group, an equivalent amount of 0.9% sodium chloride, USP (Hospira, Inc. Lake Forest, USA) was injected.

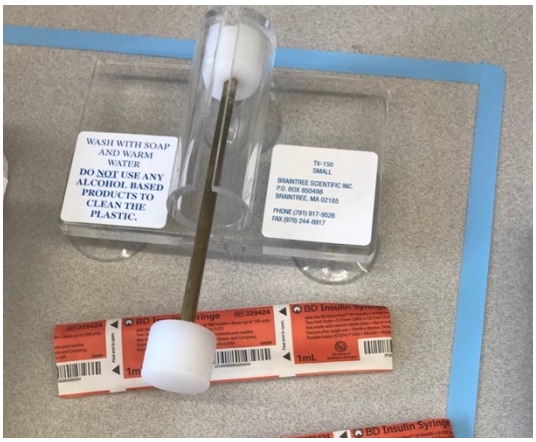

Figure 4: Immobilization device for mice' tail intravenous injection

Since there was a time gap between the injection of papaverine and oxygen micro-bubbles, mice were put back into their cages where food and hydrating gel were provided. Twenty-nine minutes after the administration of papaverine, the mouse was then measured with diffuse optical spectrometer（T=29 minutes). The mouse was then given EF5, an IHC hypoxia marker, (80 mg/Kg, IP) after the measurement (T=30 minute). The solution of EF5 was carefully light blocked during the procedure owing to its light sensitive nature. Intraperitoneal administrations were conducted through 1-mL syringe

(BD, Franklin Lakes, NJ, USA). The mouse was then put back into its cage while waiting for the next treatment. The mouse was anesthetized with 1.5% isoflurane (VIP3000 Isoflurane, Matrx, NY, USA) in the XGI-8 gas anesthesia system (XENOGEN, Alameda, CA, USA) fifty minutes after the administration of EF5 in order to have enough time to set up for the injection of oxygen micro-bubbles later (T=80). The mouse was moved from the chamber and kept anesthetized through the nose cone once it was fully anesthetized and a new tissue was placed on the heating pad. The mouse was kept prone on a tissue on top of a heating pad to maintain its body temperature during the administration and measurements. A small animal ultrasound imaging scanner (Visual Sonics Toronto, ON, Canada) was placed on the flank tumor with the Zenoscope. Sensors of both the ultrasound system and optical spectrometer were well stabilized with additional support devices. For better stabilization, the mouse was also taped in place: one over the body, one over the toes on the right side, and another over its tail. The set-up is illustrated in Figure 5.

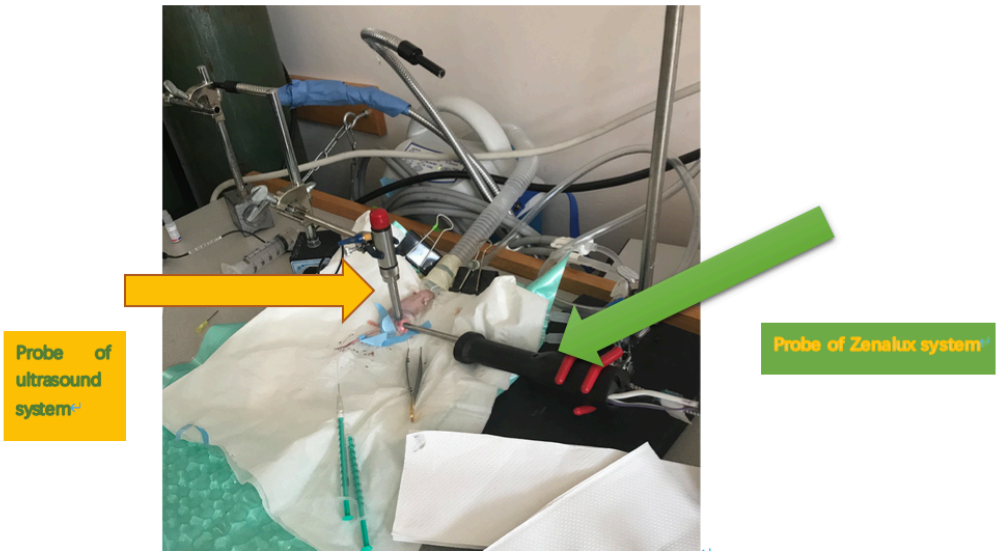

Figure 5: The actual set up for the administration of oxygen micro-bubbles and hemoglobin saturation measurement. The mouse was taped down to the tissue with three tapes. One over its tail, one over its body and another one on its toes on the right side.

The mouse was then measured multiple times for a relatively stable baseline of hemoglobin saturation. The oxygen micro-bubbles were injected into the tail intravenously 90 minutes after the administration of papaverine (T=90 minute). Hemoglobin saturation was measured continuously for 10 minutes at 15 second intervals starting from the injection of OMBs (T=90-100 minute). The completion of the Hb sat measurement was the endpoint. All mice were sacrificed via Euthosal, and their tumors were harvested for further histology study. (T=100 minutes) The tumor was removed once the mouse is confirmed dead through pinching its toes and cut through its trachea and diaphragm as a secondary form of euthanasia. All tumors were weighted and labeled accordingly once removed. Removed tumors were then flash frozen with

liquid nitrogen for histology. The timeline of all four subgroups is shown in Figure 6.

Detailed process for all subgroups is shown in Table 1.

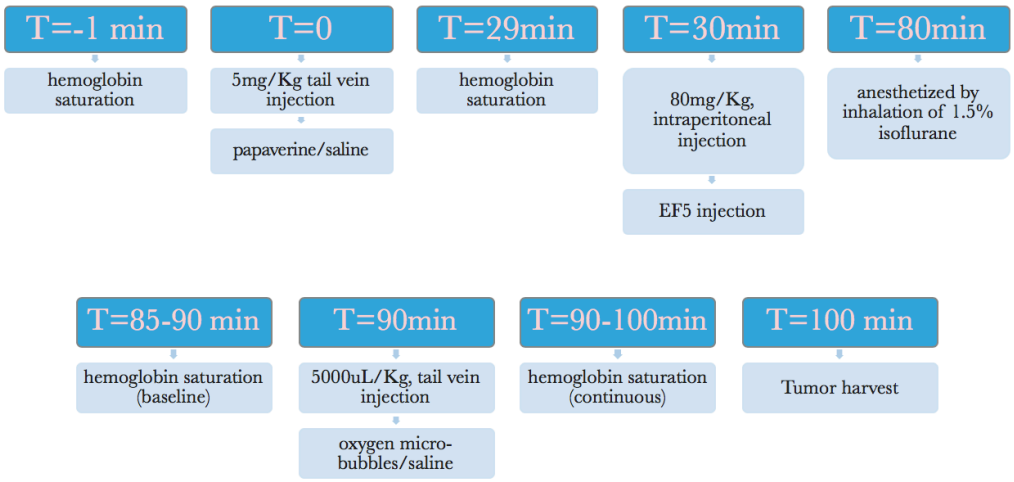

Figure 6: The timeline of the non-irradiated study

Table 1: Detailed Procedures for All Four Groups of the Non-irradiated Study

GROUP	OMB&PPV	OMB	PPV	VEHICLE
T= -1 MIN	Measure the hemoglobin saturation			
T= 0 MIN	PPV injection	Saline injection	PPV injection	Saline injection
T= 29 MIN	Measure the hemoglobin saturation			
T= 30 MIN	EF5 injection			
T= 80 MIN	Anesthetize mice with 1.5% isoflurane			
T= 85-90 MIN	Measure the hemoglobin saturation multiple times for baseline			
T= 90 MIN	OMB injection		Vehicle injection	

T= 90-100 MIN	Measure the hemoglobin saturation continuously
T= 100 MIN	Harvest tumors

2.2.3.1 Irradiated Study

Thirty-five female nu-nu mice (6-8 weeks, Duke Breeding Core) were used in irradiated study and were randomized by tumor volume into four groups once the tumor volume reached 100-200 mm^3. All experiments were performed under room temperature with a heating pad for body temperature maintenance. Mice were identified and checked through RFID chips every time for administrations and measurements. All mice were treated on the same day.

All mice were measured for hemoglobin saturation one day before the treatment (T=1 day before the treatment). First, the mouse was put into the immobilization device shown in Figure 4 and injected with papaverine (5 mg/Kg) or saline control. Since there was a time gap between the injection of papaverine and oxygen micro-bubbles, mice were put back into separate cage where food and hydrating gel were provided. The mouse was anesthetized with 1.5% isoflurane (as described above) 25 minutes after the administration of PPV in order to have enough time to set up for the injection of oxygen microbubble later (T=25 minute). The mouse was moved from the chamber and kept anesthetized through the nose cone. Once it was fully anesthetized, a new tissue is placed on the heating pad. The mouse was kept prone on a heating pad to keep them warm during the administration and irradiation afterward. A

sensor of a small animal ultrasound imaging scanner (as described above) was placed on the flank tumor which was on the right leg of the mouse. The sensor of the ultrasound system was well stabilized with additional support. The set-up for the irradiation and OMBs injection is illustrated as Figure 7.

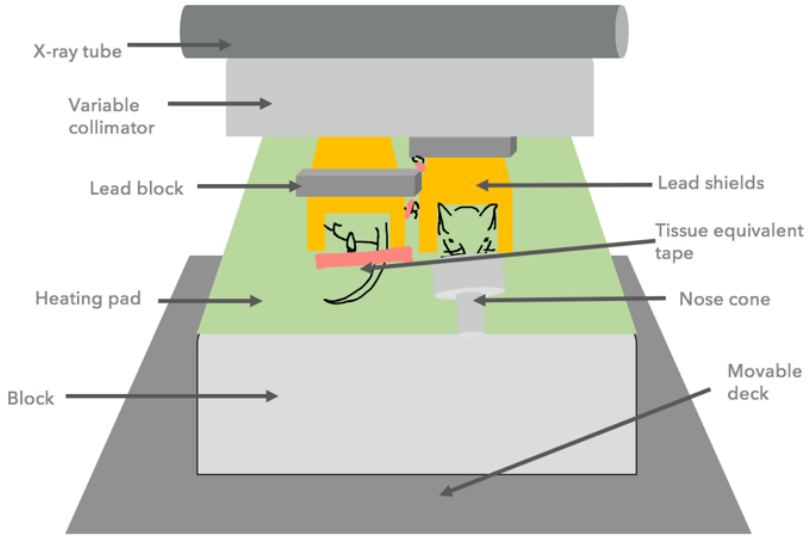

Figure 7: The overall set up in the small animal irradiator. The blocks under the heating pad (green one in the picture) was dedicated to decrease backscatter and shorten the time needed for irradiation by decrease the distance between the x-ray source and the tumor.

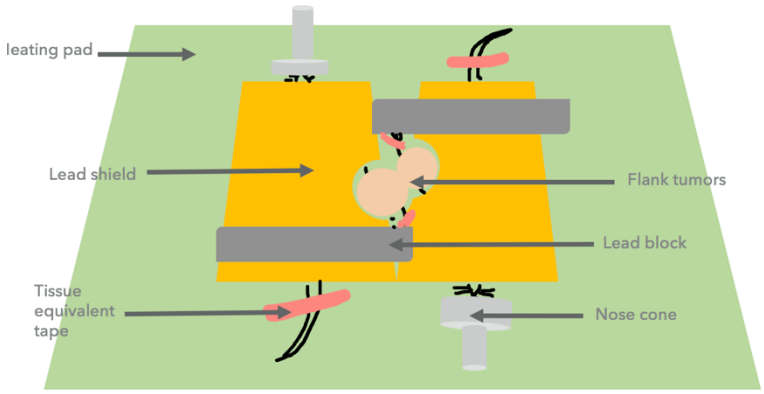

Figure 8: The set-up of mice for irradiation. To gain better dose symmetry, two mice were placed with one facing the outside (right one in the picture), the other one facing the inside (left one in the picture). Lead shields (yellow ones in the picture) were used for overall protection. Additional lead blocks (grey ones in the picture) were also used for extra protection for legs and toes. Tissue equivalent tapes, pink ones in the picture, were used for better stabilization during the treatment. There were two tapes for each mouse: one around its tail, the other one on its toes.

The oxygen micro- bubbles were injected 29 minutes after the injection of papaverine (T=29 minute) via retro-orbital injection. The ultrasound wave used for oxygen micro-bubbles triggering was applied for 60 seconds. The deck in the small animal irradiator is movable, therefore the set-up was done with the deck stick out, and then pushed back into the irradiator for irradiation which was very time efficient. Medline Aquasonic acoustic coupling gel was wiped off with Kim wipe before the irradiation, for the gel is tissue equivalent which could affect the dose distribution inside the tumor. The mouse then received a single fraction of 15Gy in the small animal irradiator (XRAD320, Precision Xray) (T= 30 minute). The mouse was then placed into separate cage for recovery after the irradiation. The mouse was returned to its cage once

regaining consciousness. All mice were monitored for their tumor growth and hemoglobin level three times a week until reaching the maximum tumor burden of 1,500 mm^3, experiencing weight loss > 15% of its original weight or developing ulcerated tumors. The timeline of the irradiated study is shown as Figure 7. The procedures for all four sub-groups in this study is illustrated in Table 2.

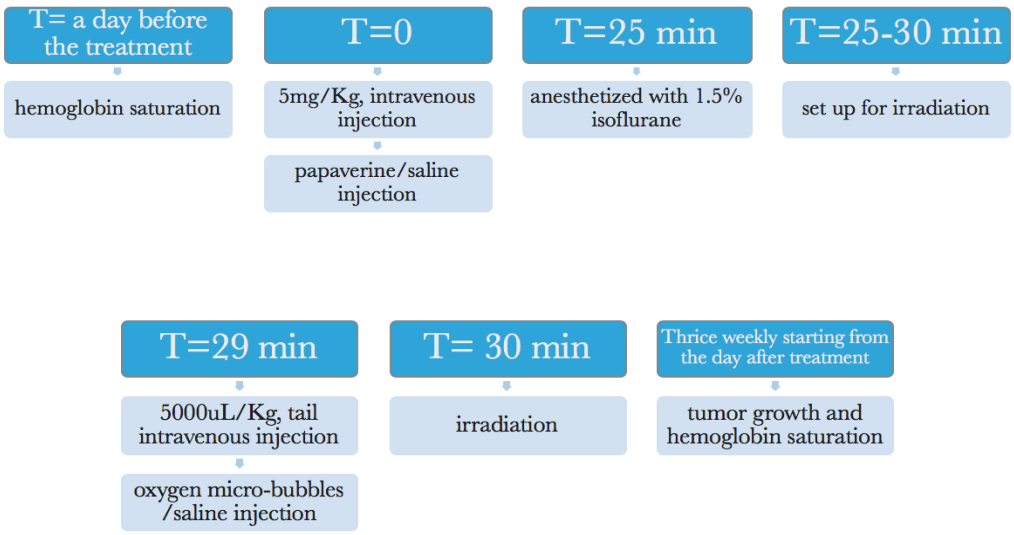

Figure 9: The timeline of the irradiated study

Table 2: Detailed Procedures for All Four Groups of the Irradiated Study

GROUP	OMB&PPV+RT	OMB+RT	PPV+RT	RT ONLY
A DAY BEFORE	Measure the hemoglobin saturation			
T= 0 MIN	PPV injection	Saline injection	PPV injection	Saline injection

T= 25 MIN	Anesthetized with 1.5% isoflurane	
T= 25-30 MIN	Set up for irradiation	
T= 29 MIN	OMB injection	Saline injection
T= 30 MIN	Irradiation	
THRICE WEEKLY	Monitoring tumor growth and hemoglobin saturation	

2.2.4 Papaverine

The papaverine was in injected solution via tail vein with concentration of 0.4 mg/mL. The tail of mouse was immersed in 38C° water to dilate the vessel in order to ease the injection. The injections were done with modified 27-gauge, 1.5-inch winged infusion catheters (Terumo, Tokyo, Japan). Polyethylene tubes (Warner Instruments, Hamden, CT, USA) were used to take the place of the original tubes. The tail of the mouse was heated with electronic warmer to help dilate the vessel. The administrations of papaverine and saline were all done when mice were awake, which is designed for minimum effect on hemoglobin saturation (Hb sat) measurements.

2.2.5 Oxygen Micro-bubbles

Oxygen microbubbles used in both the non-irradiated study and irradiated study were the exactly the same. They were made in the Borden Laboratory of the Department of Materials Science and Engineering at University of Colorado Boulder. For this experiment, a newer formulation of OMBs, DBPC C22 was used. DBPC C22 OMBs had

phospholipid shells with polyethylene glycol (PEG) brushes that encapsulated pure oxygen as core gases. For better stability and circulation persistence of perfluorocarbon gases, longer acyl-chain phospholipids were used.

Apart from that, these microbubbles were tested for irradiated stability by imaging the mouse kidney before this experiment followed by size-selecting. Differential centrifugation was used for OMBs' size-selecting. OMBs were diluted to 30 mL with oxygen saturated PBS and centrifuged at 130 relative centrifugal force to wash out OMB that were smaller than 2 μm diameter. By placing the small animal ultrasound with acoustic coupling gel directly on the shaved kidney region, the oscillation of the oxygen micro-bubbles could be observered via ultrasound. Concentrated OMB were kept in 12-mL syringe (Covidien Monoject, Mansfield, MA, USA) and shipped on the day of experiment.

For the administration of oxygen microbubbles, a VisualSonics Vevo 2100 small animal ultrasound imaging scanner (Toronto, ON, Canada) with an MS250, 18-MHa transducer at 10% power was placed on the flank tumor on the right leg of the mouse. Medline Aquasonic acoustic coupling gel was used. Mice from the OMB&PPV group (OMB&PPV+RT) and OMB (OMB+RT) group received oxygen micro-bubbles injections in random order. 5 000 μL/Kg of concentrated OMBs were injected intravenously over 60 seconds. The OMBs injection, ultrasound wave application, and hemoglobin saturation measurement were started at the same time. The injections were slow and

usually take about 40 seconds, while the ultrasound wave was applied for exactly 1 minute.

For the non-irradiated study, the tail intravenous injections were done with the same modified catheters used in the papaverine treatment. However, for the irradiated study, due to the technical difficulties of tail intravenous injection, only mice from the RT only group were injected oxygen micro-bubbles through tail veins, others were using retroorbital injection. For tail intravenous injection, the administration was exactly the same as that of the non-irradiated study using the same modified catheters. The retroorbital injection was preformed through 1-mL TB syringe, slip tip with BD PrecisionGlide™ needle (BD, Franklin Lakes, NJ, USA) which was 27 gauge, 0.5 in hypodermic. The mouse was anesthetized through nose cone. The mouse was placed in its right lateral side and a right-handed operator did the administration while other personnel held the mouse by hand. By gently squeezing the mouse 's skin on both ventral and dorsal sides to its eye in order to make its eye protruded. The needle was placed bevel down at around 30° and inserted into the medial canthus.

2.2.6 Quantitative Optical Spectroscopy

The hemoglobin saturation measurements were all through the usage of a diffuse optical spectrometer. The spectrometer was calibrated each time before uses.

For the non-irradiated study, the measurement at T= -1 minute and T= 29 minute were both one-time measurement with the probe placed directly on the surface of the

flank tumor. The probed should be in firm contact with the mouse's skin while not put much pressure on its leg in order to avoid damage to the mouse. The measurement that took place at T= 85-90 minutes was used for determining Hb sat baseline. At T= 90-100 minutes, hemoglobin saturation was measured for ten minutes at 15 second intervals.

For the irradiated study, because the tumor volume developed with time, in order to present a more comprehensive measurement, each percent hemoglobin saturation was the average of three measurements starting eleven days after the treatment. All three measurements were taken at three random places on the tumor in relative short period of time.

2.2.7 Radiation Therapy

Thirty-four mice were irradiated with a single fraction of 15 Gy for one of the mice from the RT only group dead during the administration of papaverine due to stress response. The radiation was conducted in the small animal irradiator described above. The dosimetry was conducted one day before the treatment. The set-up for dosimetry was exactly the same as the actual treatment, as illustrated in Figure 7. The dosimetry for tumors is shown in the Table 3. The average dose rate of the treated and non-treated mice was 7.2 cGy/sec based on the average of the thrice measurements. Therefore, in order to deliver 15 Gy (1500cGy) to the tumor, the Precision Xray X-RAD 320 was set to 320 kv, 10mA, with F1 filter（2.0mm Aluminum, HVL=1.0mm Cu）located between the tube and collimator.

Table 3: The Dosimetry for Irradiated Study

GROUP	OMB&PPV+RT, OMB+RT	PPV+RT, RT ONLY
DOSE1 (CGY) OVER 30 SEC	218.52	218.56
DOSE 2 (CGY) OVER 30 SEC	217.32	215.69
DOSE 3（CGY）OVER 30 SEC	216.86	213.48
AVERAGE OVER 30 SEC	217.567	215.91
OVERALL AVERAGE OVER 30 SEC	216.74 with stand deviation of 1.93	

2.3. Results

2.3.1 Hemoglobin Saturation for the Non-irradiated Groups

2.3.1.1 Oxygen Micro-bubbles Induced Hemoglobin Changes

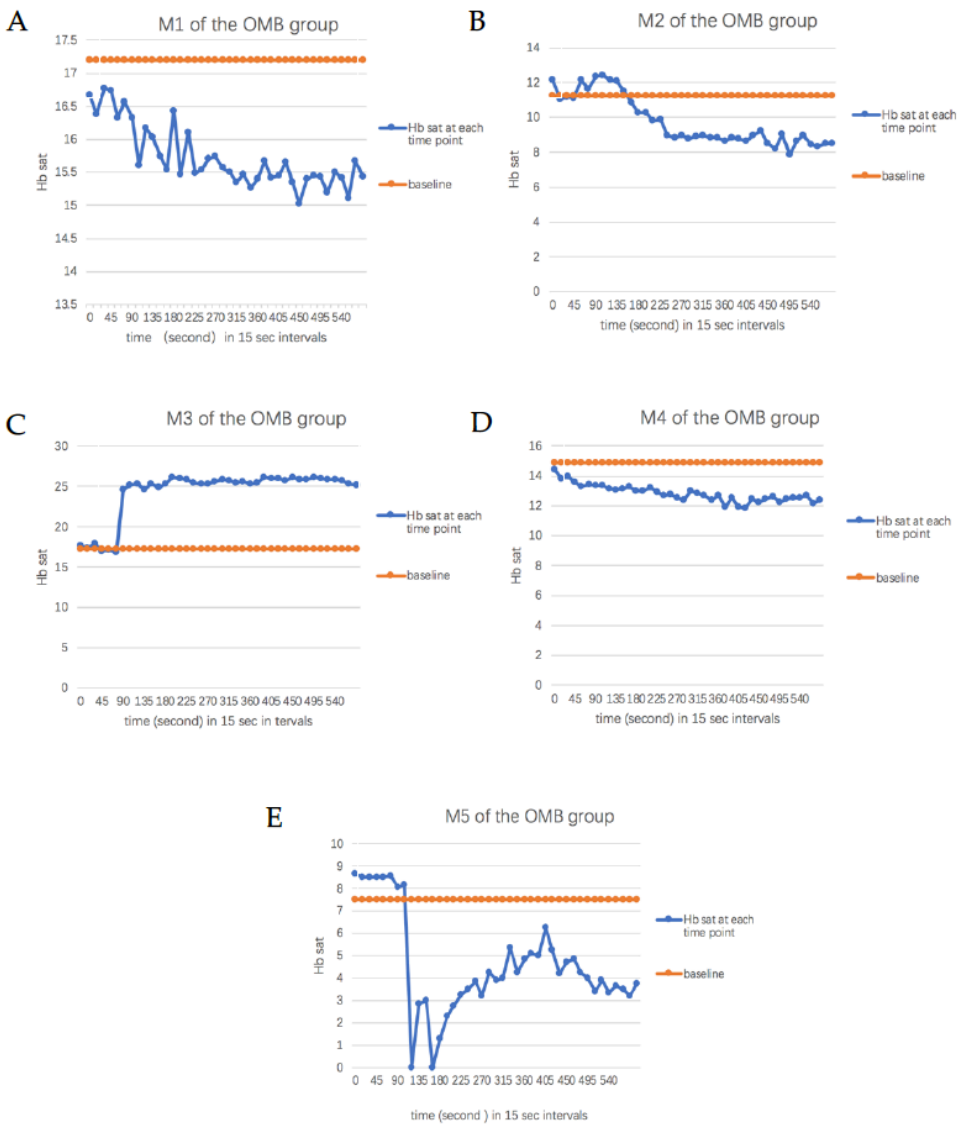

Figure 10: The changes of hemoglobin saturation in comparison of the baseline with the injection of oxygen micro-bubbles for the OMB group. The changes of Hb sat for (A) M1; (B) M2; (C) M3; (D) M4; and (E) M5. The baseline is the average of several individual measurements that are within 10% offset. The hemoglobin curve is a continuous measurement.Three out of five mice show an increase in Hb saturation with the OMBs administration.

Five mice from OMB group showed heterogenous responses to the administration of oxygen micro-bubbles. Three of them (M2, M3, and M5) show an initial increase from baseline followed by a decrease (M2 and M5) or a constant increase (M3) (Figure 8). M2 shows a little increase with fluctuation compared with the baseline at about 50 seconds starting from the administration which sustained about 1 minute. The following hemoglobin saturation level is lower than the baseline and relative stable with little fluctuations. M3 shows considerable improvement of percent hemoglobin saturation at about 90 seconds starting with the administration and stay so for the rest of the 490 seconds until the end of the measurement. M5 shows a higher level of hemoglobin saturation at the very beginning with the administration and drops very fast to zero at about 110 seconds. The curve of M1 seems to be undulant, and it is lower than the baseline the whole time. The curve of M4 is relatively stable and is always lower than the baseline. Noticeably, three out of five mice have showed a noticeable offset of the baseline and the Hb sat level at the beginning of the administration of oxygen micro bubbles. Four of the mice have a descending changing curve overall.

Figure 11: The changes of hemoglobin saturation in comparison of the baseline with the injection of oxygen micro-bubbles for the OMB&PPV group. The changes of Hb sat for (A) M1; (B) M2; (C) M3; (D) M4; and (E) M5.The baseline is the average of serval individual measurements that are within 10% offset. The hemoglobin curve is a continuous measurement. Three out of five mice show an increasement with the administration of OMBs

Responses of the five mice are relatively heterogeneous, Three mice of the OMB&PPV group, M1, M2, and M3, shows in increase from baseline. M1 shows an increase right at the beginning of the administration, and it lasts about 180 seconds. It should be noted that the baseline of M1 is much higher compared with other mice in this group. The percent hemoglobin saturation of M2 increases at about 45 seconds and is maintained for the rest of the measurement. The curve of M3 is higher than its baseline at the beginning, increases at about 90 seconds, and keeps increasing for the rest of the measurement. M4 and M5 show the same fluctuant pattern of decline. Three of them show sizable offset at the very beginning. Two of them show clear decline overall. Two of them seem to have showed periodical fluctuations.

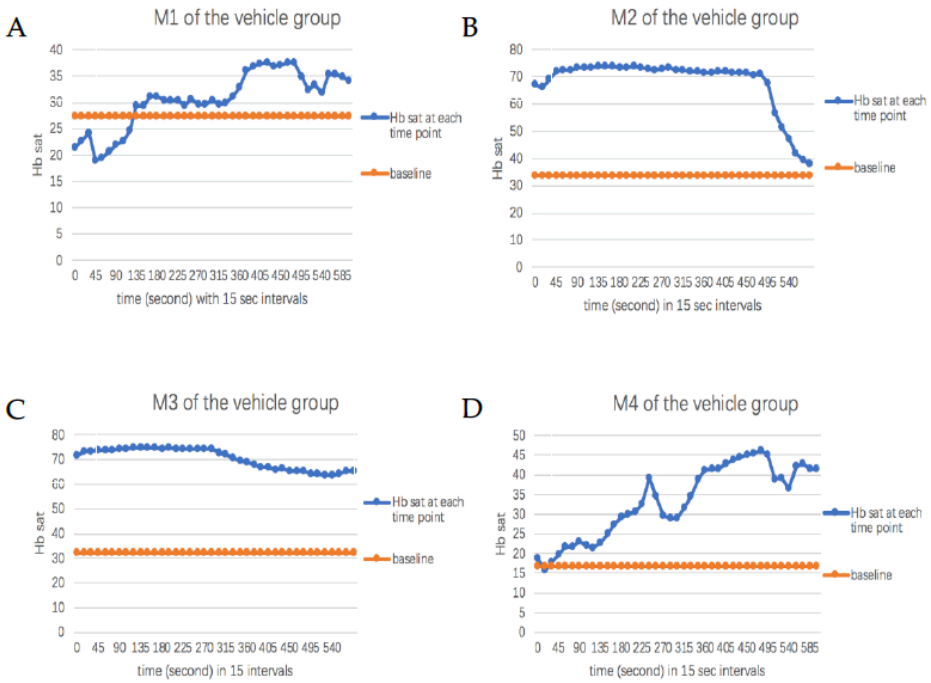

Figure 12: The changes of hemoglobin saturation in comparison of the baseline with the injection of oxygen micro-bubbles for the OMB&PPV group. The changes of Hb sat for (A) M1; (B) M2; (C) M3; and (D) M4. The baseline is the average of serval induvial measurements that are within 10% offset. The hemoglobin curve is a continuous measurement. Four out of four show an increase with the administration of saline

All four mice of the vehicle group have showed higher level of hemoglobin saturation compared with baseline. M1 and M4 have showed relatively undulant changes during the measurement. M2 and M3, on the other hand, showed rather stable changes over the treatment. Notice that three out of four have showed substantial offset right at the beginning, especially for M2 and M3, the differences are as large as 40% at the same time of the administration.

2.3.1.2 PPV Induced Hemoglobin Changes

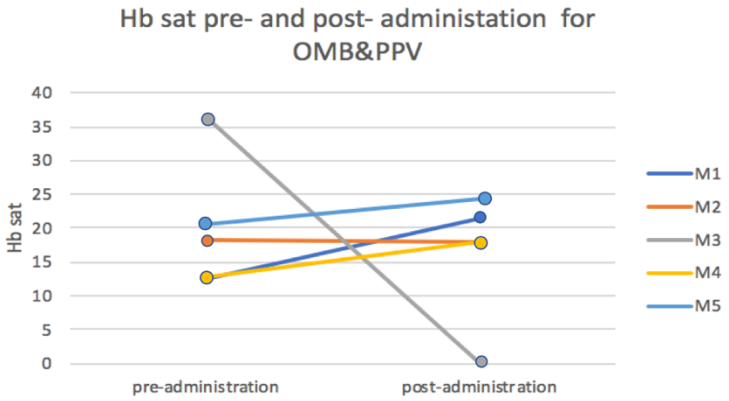

Figure 13: Individual data points demonstrating the percent hemoglobin saturation before and 29 minutes after the administration of papaverine for the OMB&PPV group. Individual points represent pre- and post-administration values

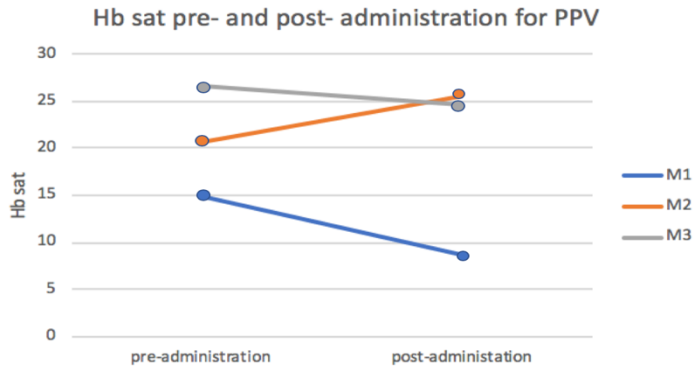

Figure 14: Individual data points demonstrating the percent hemoglobin saturation before and 29 minutes after the administration of papaverine for the PPV group. Two pre-administration data were missing due to correction problem. Individual points represent pre- and post-administration values

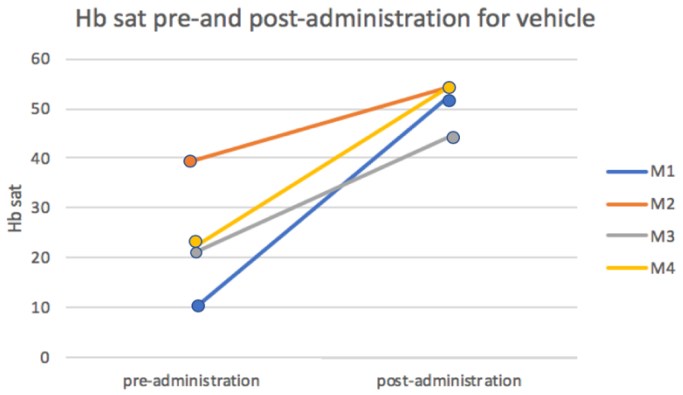

Figure 15: Individual data points demonstrating the percent hemoglobin saturation before and 29 minutes after the administration of papaverine for the vehicle group. Individual points represent pre- and post-administration values

The combined OMB &PPV group (Figure 13) has three out of five mice that showed an increase of Hb sat after the injection of papaverine. While only one out of three in the PPV group showed an increase compared to baseline (Figure 14). There are only three mice included in Figure 14 due to missing measurements. However, all four mice from the vehicle group showed apparent increase after the saline injection (Figure 15).

2.3.1.3 Oxygen Micro-bubbles and Papaverine Induced Hemoglobin Changes

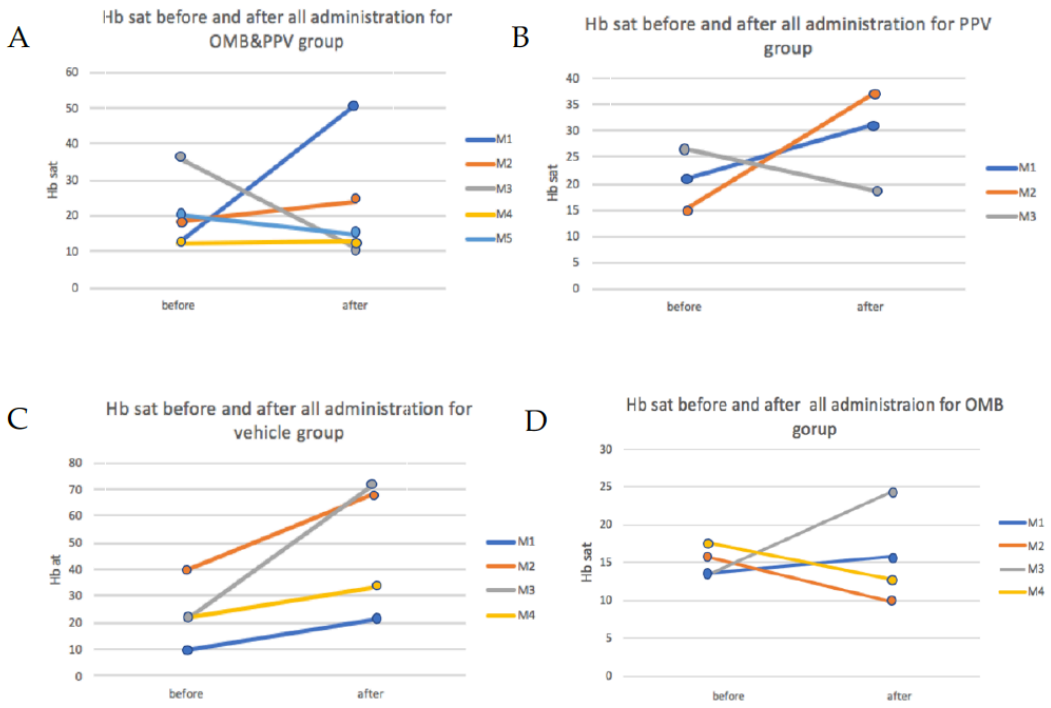

Figure 16: The percent hemoglobin saturation changes with administration of oxygen microbubbles, papaverine and or equivalent amount of saline. The Hb sat before and after all treatment for (A) OMB&PPV group; (B) PPV group; (C) vehicle group; (D) OMB group. Individual points represent pre- and post-administration values

Two out of five mice from the OMB&PPV+RT group show an increase in percent hemoglobin saturation. Two out of three mice in the papaverine group have higher value of percent hemoglobin saturation after the administration of papaverine and saline. Two out of four mice in the oxygen micro-bubbles group have an increased value of percent hemoglobin saturation value post-administration of OMB and saline. However, all four mice from the saline group show increased Hb sat after saline

injection. None of the experiment groups demonstrate improved level of oxygenation compared with the control group. Among them, OMB&PPV group is the least effective in improving hemoglobin saturation.

2.3.2 Radiation Outcome and Oxygenation for the Irradiated Groups

2.3.2.1 Radiation Outcome

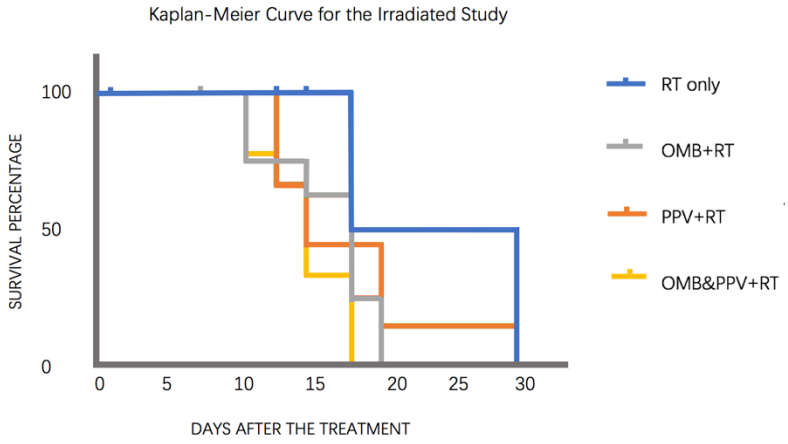

Figure 17: The survival curve for the irradiated study

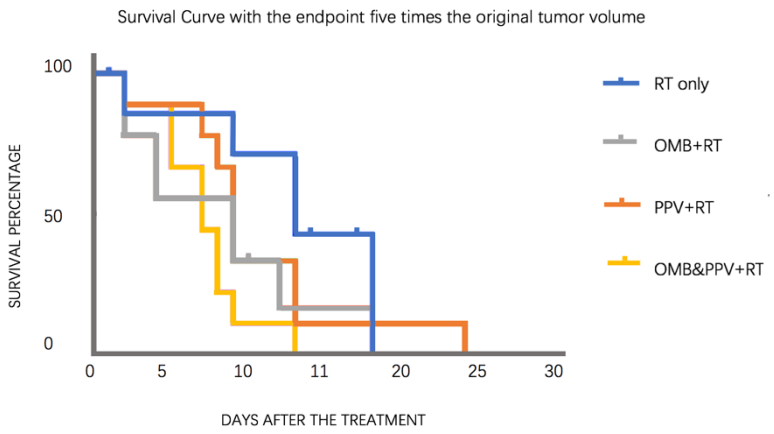

Figure 18: The survival curve with the endpoint of five times the original tumor volume

Tumor control rate seems to be better in the RT only and PPV+RT group. (Noticeably, the RT only group has the smallest number of mice in all four groups.) However, the RT only group has the most complications due to ulceration and weight lost, while the OMB&PPV+RT has none. The following graph demonstrate the comparison of complication among different groups

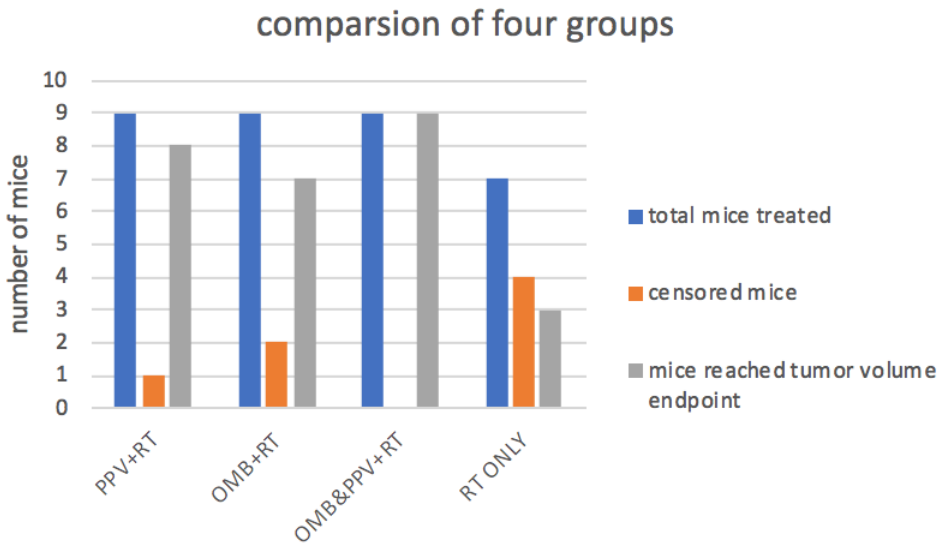

Figure 19: The number of censored mice and the ones that reached endpoint for all four groups in the irradiated study

This figure demonstrates the number of mice censored in each group. In this study, mice were censored for two reasons: 1) significant decrease in weight (> 15%); 2) an ulcerated tumor that was less than 1 500mm^3. Not that in the RT only group, three mice were censored due to ulceration, while one was censored for weight lost. In the remaining groups, two were censored due to ulceration in the OMB+RT group, one was censored due to ulceration in the PPV+RT group, and none were censored in the OMB&PPV+RT group.

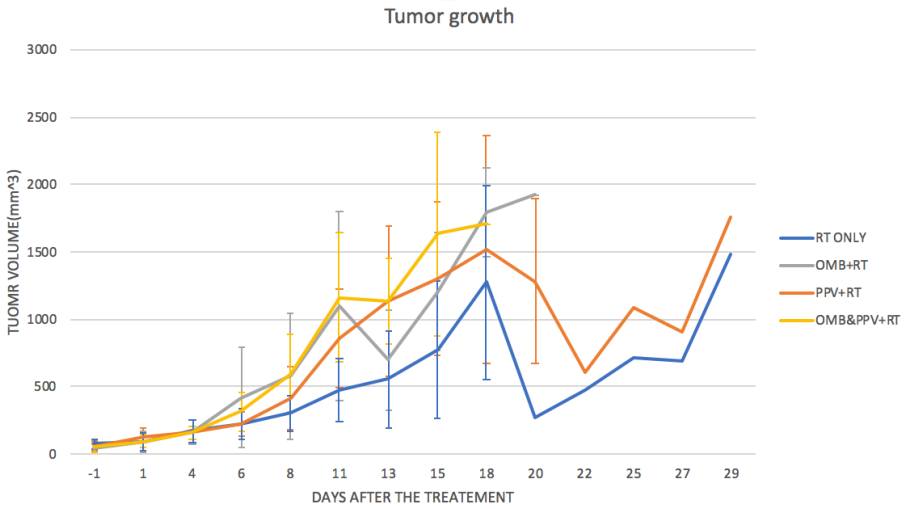

Figure 20: The graph demonstrating the tumor growth include all mice of the irradiated study. The mean and standard deviation are shown above

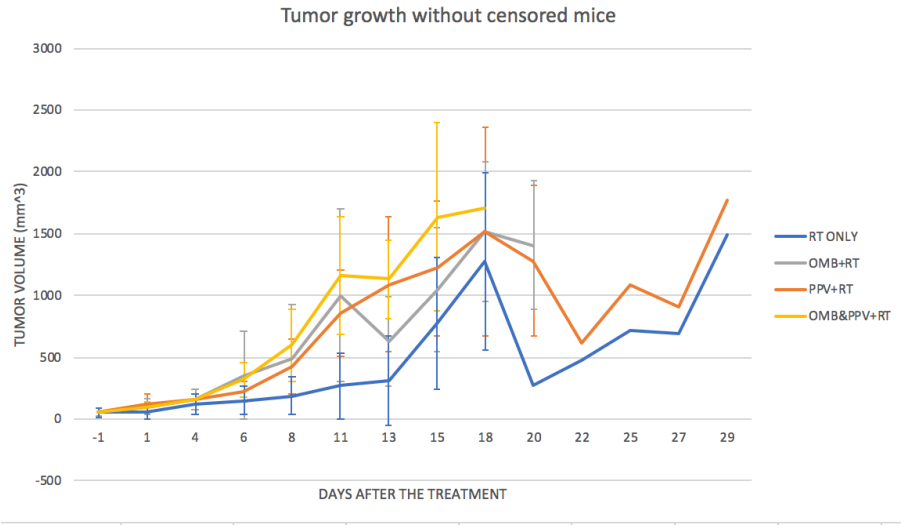

Figure 21: The graph demonstrating the tumor growth include all mice of the irradiated study excluding the censored mice. The mean and standard deviation are shown above

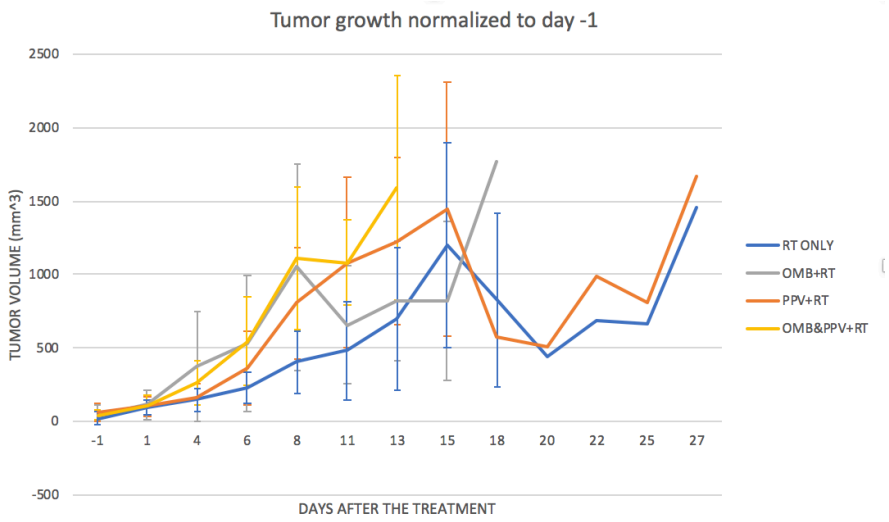

Figure 22: The graph demonstrating the tumor growth include all mice (excluding censored mice) of the irradiated study normalized to day one. The mean and standard deviation are shown above

There is only one mouse from the RT only group and one from the PPV+RT group survived after day 18. There is no significant improvement in tumor control for the OMB&PPV+RT group.

2.3.2.2 Percent Hemoglobin Saturation Changes

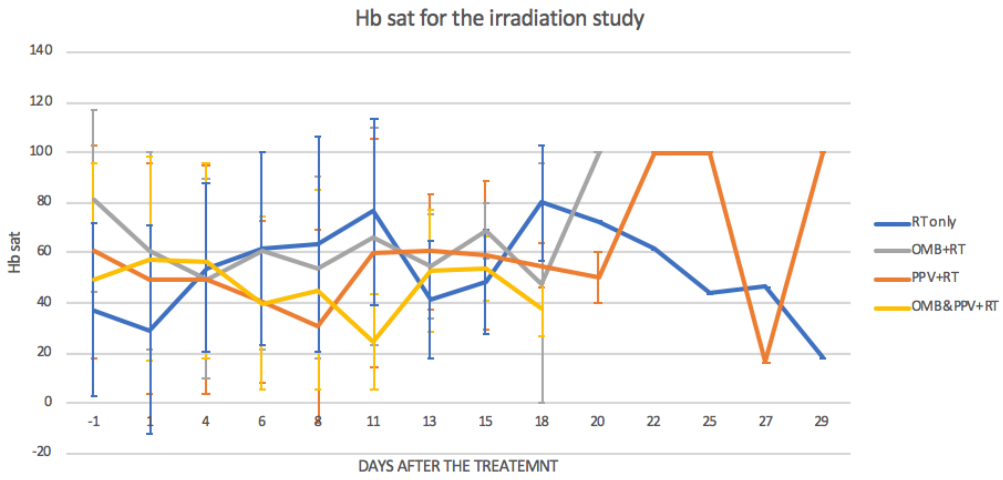

Figure 23: The graph demonstrating the percent hemoglobin saturation changes include all mice of the irradiated study. The mean and standard deviation are shown above

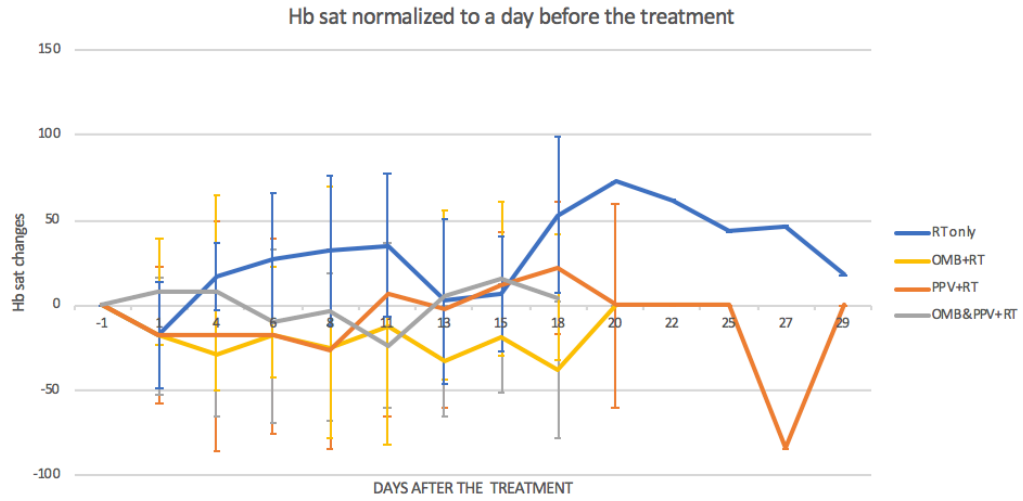

Figure 24: The graph demonstrating the percent hemoglobin saturation changes for all mice of the irradiated study normalized to the day before the treatment. The mean and standard deviation are shown above

The Figure 23 and Figure 24 demonstrate the percent hemoglobin saturation changes for all mice until they reach the tumor burden volume or have to be censored

due to ulcerated tumors. Starting from day 11, the percent hemoglobin saturation level represents the average of three seperate measurements with development of the tumor volumes. It seems the Hb sat changes are rather heterogeneous across four groups. Interestingly, only the OMB&PPV+RT group showed increased Hb sat level a day after the treatment, while all other groups: PPV+RT, OMB+RT, RT only groups showed decreased Hb sat level compared with the day before the treatment.

The percent hemoglobin saturation changes with the administration of oxygen micro-bubbles and/or papaverine, or saline appear to be heterogenous between and within each group for the non-irradiated study (Figure 10-15). Neither the combined nor the separate administration of oxygen micro-bubbles or papaverine have shown advantages in improving tumor oxygenation compared with the vehicle group based on measurements from a diffuse optical spectrometer (Figure 16).

Based on the overall survival rate, neither the combination nor the separate administration oxygen micro-bubbles and papaverine shows a positive effect as a radiosensitizer (Figure 17,18). However, the combination of oxygen micro-bubbles and papaverine may have offered some radioprotective effect for normal tissue compared with OMB+RT, PPV+RT and RT only (Figure 19) for it is the group with the fewest censored mice. Some improvements can also be observed from the percent hemoglobin saturation of the OMB&PPV+RT group the day after the treatment compared with the day before the treatment, and it is the only group that showed an increase (Figure 24).

2.4. Discussion

There have been various strategies proposed for the sensitization of tumor hypoxia. One approach is through increasing the oxygen supply to the hypoxic cancerous tissue, while an alternative way is targeting tumors' metabolic demand for oxygen. In this work, we studied the combined effects of oxygen micro-bubbles and papaverine in alleviating hypoxia in a mouse KP sarcoma model and in improving radiation therapeutic ratio. The presented data did not show positive results of the combination effect of oxygen micro-bubbles and papaverine in universally increasing the Hb sat level for the non-irradiated study nor in improving RT tumor control for the irradiated study. However, the Hb sat level measurement shows improvement the day after the treatment only for the OMB&PPV+RT group. Apart from that, the combination may have offered some protective effect for the normal tissue after the radiation therapy. The reason that this study failed to demonstrate oxygen micro-bubbles and papaverine to be effective in functioning as a sensitizer to RT by alleviating hypoxia in mouse KP sarcoma model based on current data still remains unclear. The following are some practical and theoretic limitations that might contributed to this negative result.

From a practical perspective, for the non-irradiated study, the main limitations lie in the hemoglobin measurement. First of all, the individual measured hemoglobin level for different time points may not be representative of the oxygenation level at exactly the same spot despite a small tumor burden. Second of all, the measured

hemoglobin level does not represent overall oxygenation at the measured spot owing to the time varying nature of tumor hypoxia, which is well illustrated in Figure 8,9 and 10. As Hu *et al.* has demonstrated, the oxygenation kinetics differ between tumors.[49] Therefore, the Hb sat measurement is not sufficient to characterize hypoxia adequately even though it is the standard way to indirectly measure hypoxia. Long term monitoring would offer more comprehensive data. However, it is worth mentioning that would require a good deal of staffing and equipment in order to treat all mice on the same day. This is critical because the tumor volume would vary significantly with just a day's difference based on our data. Apart from that, the baseline for the oxygen micro-bubbles administration were individual measurements that were collected intensively over a relatively short period of time and in a single location. This may not be enough since there were some mice that showed a sizable off-set of hemoglobin saturation at same time of administration, especially for the vehicle group. Therefore, monitoring physiological parameters including body temperature, heart rate, pH level and breathing rate is also of great importance for the evaluation of the oxygenation levels owing to their impact on hemoglobin saturation. For example, with the increase of temperature, the oxygen dissociation curve will shift to its right side and reduce the percent of oxyhemoglobin. Apart from that, pH level also plays a significant role in shifting of the oxygen dissociation curve while has known effect on the level of 2,3-diphosphoglycerate (2,3-DPG), which is an important factor for hemoglobin function.[66]

For the radiation study, there were still dose differences between the OMB-injected groups and non-OMB-injected groups although the irradiation set up was carefully designed and tested. There was a 0.1143 Gy difference for the single fraction of 15 Gy irradiation. The step of wiping the acoustic coupling gel from the flank tumor before treatment with x-ray was carried out carefully throughout the experiment. However, the effectiveness of both oxygen micro-bubbles and papaverine are highly related with time. Time is a significant factor to be considered during the experiment. It was a practical dilemma to remove the gel efficiently within the time limit. Due to the limited ability in regulating temperature of nu-nu mice, other more effective cleansers, for example alcohol, were not used for the removal. The residual gel, which is nearly water equivalent, may act as a redundant bolus for the radiation treatment and change the dose distribution. Apart from that, though aiming for subcutaneous tumor models, the KP sarcoma tumors developed in the irradiated study were more intramuscular which caused problems in the tumor measurement for it is much more difficult to find the tumor frontiers, which could affect the overall survival analysis since the endpoint used was maximum burden tumor volume. Moreover, one of the differences between this experiment and the previous study by Borden at el. which succeeded in alleviating tumor hypoxia through the usage of lipid-based oxygen micro-bubbles is that instead of directly injection into the tumors,[50] they were injected intravenously though tail vein and retro-orbitally. This would be more feasible for fractionated treatments once applied

clinically. A more recent study conducted by Eisenbrey *et al.* showed an increase in hemoglobin saturation levels in murine breast cancer model using lyophilized surfactant shelled oxygen micro-bubbles ($SE61O_2$). [65] However, the optimized oxygen retention might remain too short for the ultrasound release even though an improved formula was used. Repeating with intratumoral injection would be another potential step.

From a theoretical perspective, complex physiologic mechanisms are involved in oxygenation in cancerous tissue. Previous successful attempts to test the effect of papaverine on improving radiation index were in rodent E0771 or A549 models,[13] which could indicate papaverine's ability to increase tumor oxygenation is dependent on the tumor model. In addition, the increase in oxygen supply and the stress the mice underwent during the administration and irradiation may cause tumor arteriolar vasoconstriction, therefore reducing the overall blood flow in tumor. This decrease in tumor perfusion could have outweighed the increase in oxygen supply of the blood. Additionally, red blood cells, as the main way to transport oxygen in vertebrates, might already be at their maximum capacity at the time of administration for they were breathing 100% O_2 and thereby reflected no significant increase in Hb sat. Besides, the poorly formed vessels in the cancerous tissue could be the biggest obstacle for increased oxygen delivery to the tumor region. In addation, the microbubbles might not circulate long enough or may realease their oxygen too quickly prior to reach the tumor.

With respect to the hypoxia measurement endpoint itself, one of the limitations of optical spectrometer is the penetration depth. It would be preferred if the modality could penetrate deeper into the tumor in order to offer oxygenation at various spatial locations and provide a tumor map with Hb sat at multiple places. Apart from that, as an indirect measuring device for hypoxia, diffuse optical spectrometer is dependent on blood perfusion, and cannot provide the concentration of dissolved oxygen in the intercellular space directly, instead it can only demonstrate the oxygen delivery in the vasculature. It should also be noted that even though Complex I inhibitor may cause tumor growth arrest, there are certain mutations in mitochondrial DNA that can lead to pro-tumorigenic effects.[58] The self-contradictory effect of Complex I could cause its effect to vary with type and severity of oxidative phosphorylation dysfunction. [59] Cruz-Bermúdez *et al.* showed that cancer cells with ND4 or ND6 mutations could cause mild increase in tumor size in nude mice model.[60] Interestingly, Li *et al*. have demonstrated that Complex I may have negative impact on the mitochondrial permeability transition pore which is responsible for apoptosis and necrosis. [61] Therefore, an inhibitor of Complex I may result in apoptosis.[60] In addition, mutations in ND5 would lead to a higher tumorigenic potential.[62]

3. Future Work

For the non-irradiated study, due to the practical and theoretical limitations of diffuse optical spectrometer, a follow-up histology study would help to provide more information of the overall oxygenation of tumors. The IHC study of EF5 could reveal the relationship between the oxygen partial pressure of the tumor tissue and blood vessel distribution, CD31 staining would provide data on the vasculature and Hoechst staining would show anatomical data.

For the irradiated study, based on current data, there might be a radioprotection effect for normal tissue of the combination of oxygen micro-bubbles and papaverine. An *in vitro* study could be the next step to help further study this. By dividing them into four groups: 1) OMB&PPV+RT; 2) OMB+RT; 3) PPV+RT; 4) RT only and measuring the reactive oxygen species (ROS), which damage DNA and causes cell death, we may further explore this potential.

It is possible that the effect of papaverine and micro-bubbles' ability to increase tumor oxygenation varies between tumor models. We may test this through another *in vivo* study by testing the pO_2 level with the administration of OMBs and PPV in different murine tumor models. Since Hb sat measurement only loosely correlated with tissue O_2. To be on the safe side, a second method would be used to confirm the baseline, for example, immunostaining of a key hypoxia marker. Apart from that, an oxylite probe could provide better point measurement. Imaging devecies like EPR, MRI may also help.

In order to gain a better radiotherapy overall, use of an image guided irradiator, and radiotherapy plan might be useful.

4. Conclusion

In this study, we investigated the combined effect of oxygen micro-bubbles and papaverine in sensitizing hypoxic tumors to radiation therapy in a mouse sarcoma model. The current study data does not have enough evidence to support the hypothesis that the combination of OMBs and PPV can alleviate tumor hypoxia and act as a radiosensitizer for radiotherapy. This could be due to certain practical and theoretic limitations of the study. However, the current data revealed that there might be a radioprotective effect for normal tissue of the combination of oxygen micro-bubbles and papaverine, which could be an interest project to be investigated in the future. Apart from that, the percent hemoglobin saturation measurement of the OMB&PPV+RT showed a modest increase the day after the radiotherapy compared with the day before the treatment, which could indicate the effect of the combination of oxygen micro-bubbles and papaverine in alleviating tumor hypoxia following radiation therapy, which could be promising for fractionated therapy if it holds true.

To further investigate the effect of oxygen micro-bubbles and papaverine, an IHC study could help reveal the oxygenation and vasculature inside the tumors. And another study of different tumor models may be of interest to see if the effect of OMBs and papaverine is different among different tumor types.

Appendix A

The tumor growth for the four groups of the irradiated study

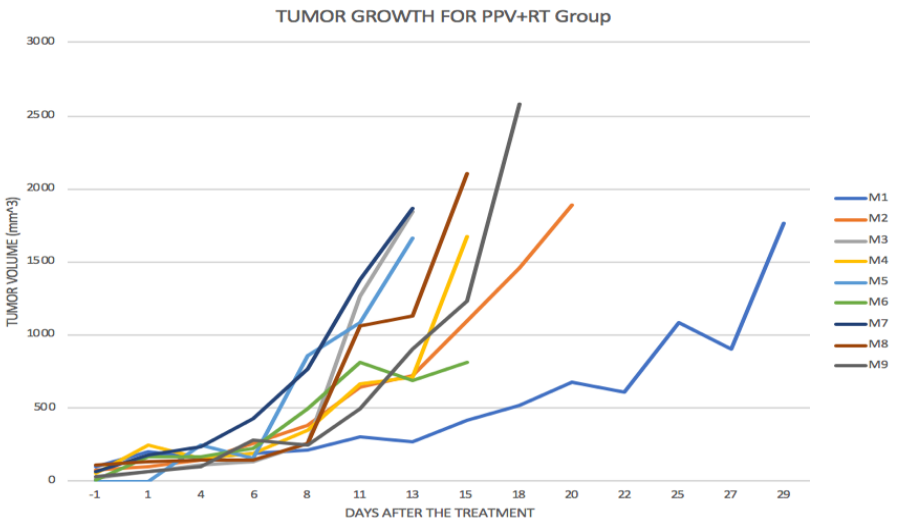

Figure 25: Tumor growth for all mice from the PPV+RT group

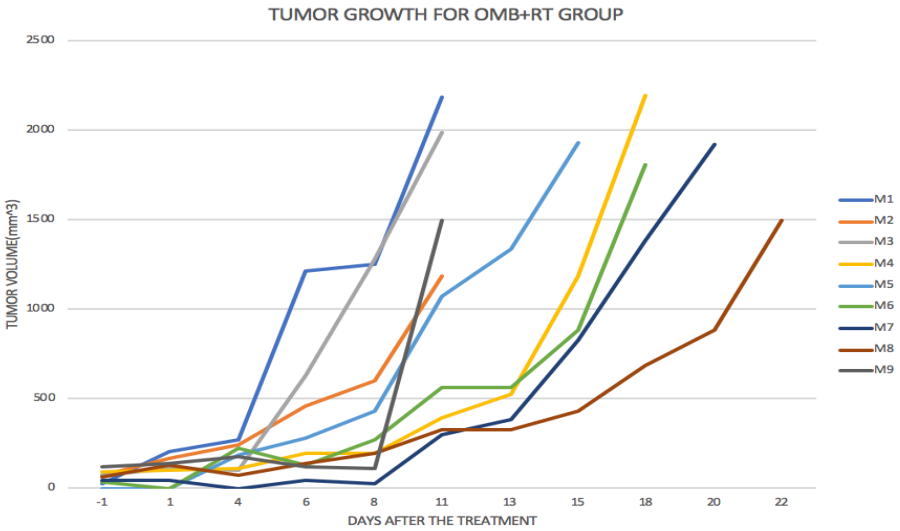

Figure 26: Tumor growth for all mice from the OMB +RT group

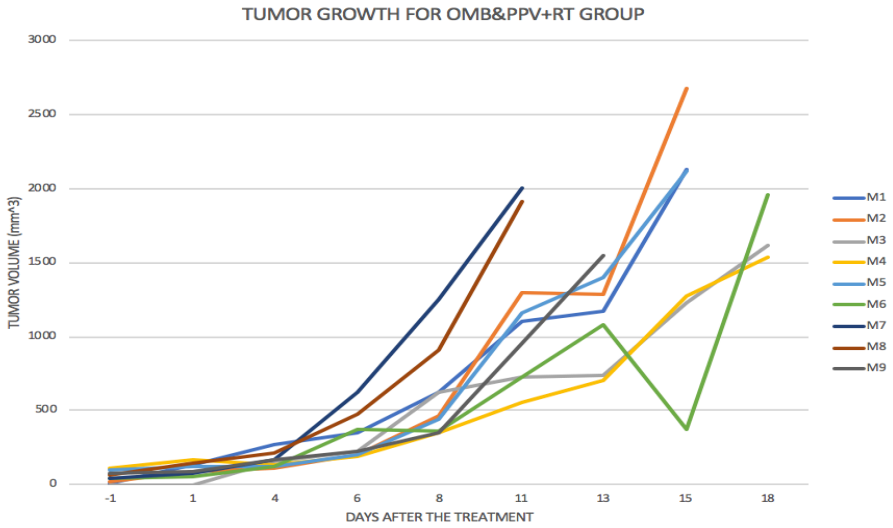

Figure 27: The tumor growth for all Mice from OMB&PPV+RT group

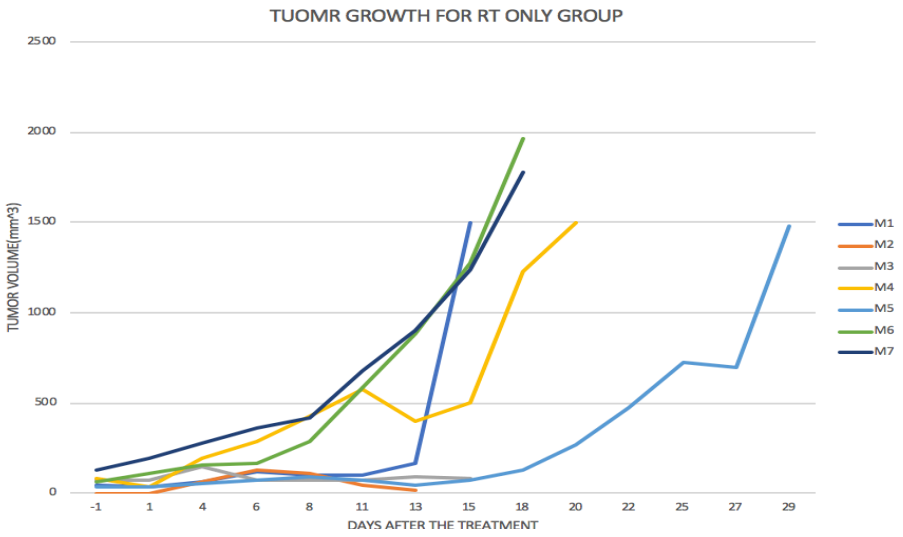

Figure 28: The tumor growth for all mice from RT Only group

The percent hemoglobin saturation changes for four groups of the irradiated study

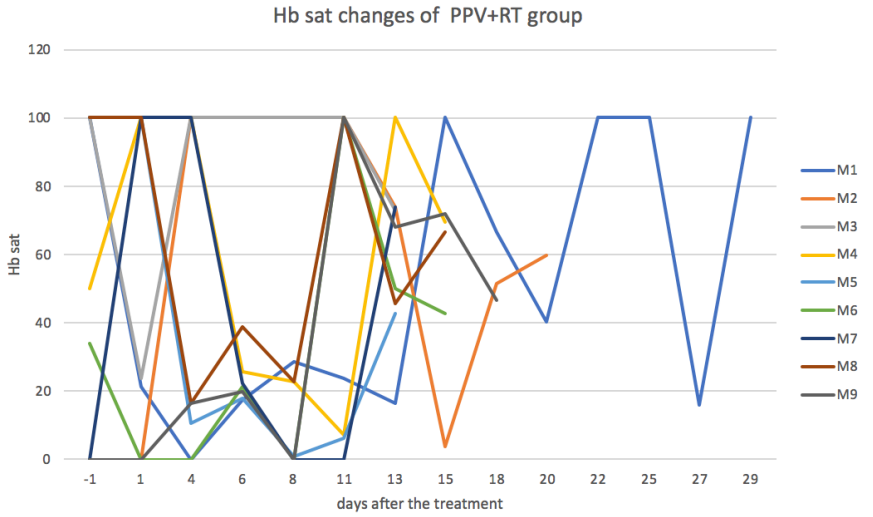

Figure 29: The percent hemoglobin saturation for all mice from the PPV+RT group

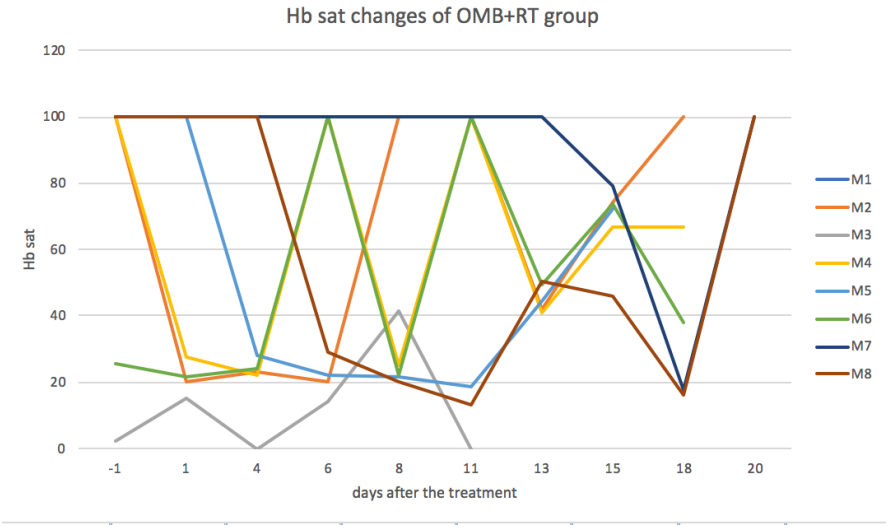

Figure 30: The percent hemoglobin saturation for all mice from the OMB+RT group

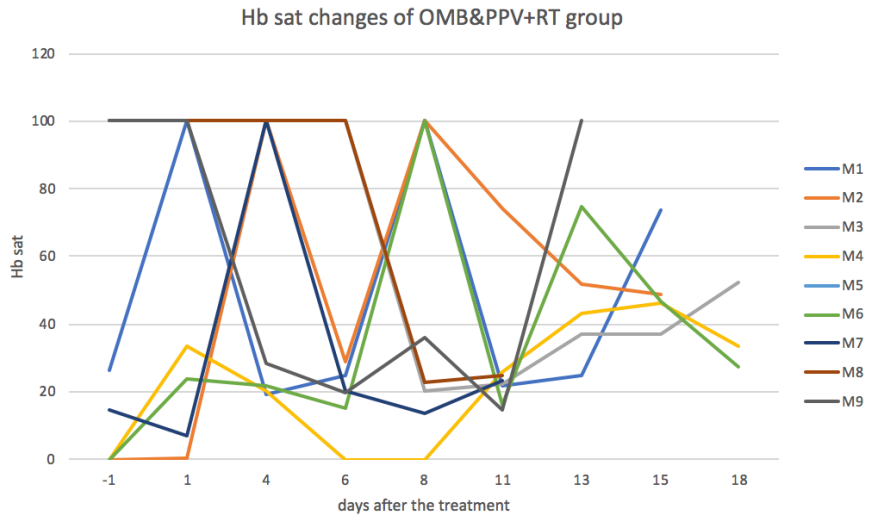

Figure 31: The percent hemoglobin saturation for all mice from the OMB&PPV+RT group

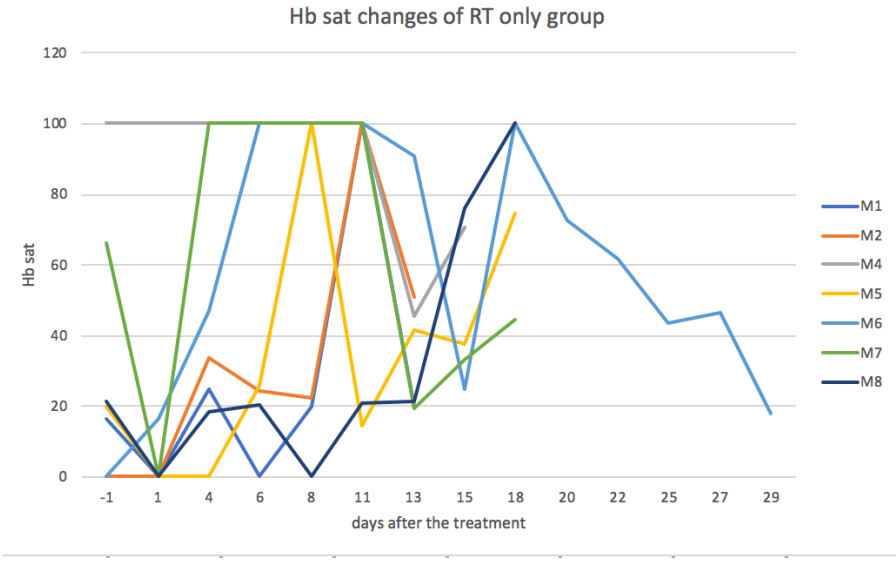

Figure 32: The percent hemoglobin saturation for all Mice from the RT Only group

References

1. Brown, J.M. & Giaccia A.J. The unique physiology of solid tumors: opportunities (and problems) for cancer therapy. *Cancer Res* 58,1408-16 (1998).

2. Epstein, T., Xu, L., Gillies, R.J. & Gatenby, R.A. Separation of metabolic supply and demand: Aerobic glycolysis as a normal physiological response to fluctuating energetic demands in the membrane. *Cancer Mol Med* 2-7 (2014).

3. Gray, L. H. et al. The concentration of oxygen dissolved in tissues at the time of irradiation as a factor in radiotherapy. *The British Journal of Radiology* 26, 638-648 (1953).

4. Semenza, G. L. The hypoxic tumor microenvironment: a driving force for breast cancer progression. *Molecular Cell Research* 1863, 382-391 (2015).

5. Evans, S. M., & Koch, C. J. Prognostic significance of tumor oxygenation in humans. *Cancer Letters* 195, 0-16 (2003).

6. Thomlinson, R. H. & Gray, L. H. The histological structure of some human lung cancers and the possible implications for radiotherapy. *Br. J. Cancer* 9, 539-549 (1955).

7. Rajamanickam, B., Ann, L. K., Richard, Y. & Kheng-Wei, Y. Cancer and radiation therapy: current advances and future directions. *International Journal of Medical Sciences* 9, 193-199 (2012).

8. Kaanders, J. H. A. M., Bussink, J. & Kogel, A. J. V. D. Clinical studies of hypoxia modification in radiotherapy. *Seminars in Radiation Oncology* 14, 233-240 (2004).

9. Dunn, T. J. *et al.* The effects of hyperoxic and hypercarbic gases on tumour blood flow. *British Journal of Cancer* 80, 117-126 (1999).

10. Mendenhall, W. M., Morris, C. G., Amdur, R. J., Mendenhall, N. P. & Siemann, D. W. Radiotherapy alone or combined with carbogen breathing for squamous cell carcinoma of the head and neck: a prospective, randomized trial. *Cancer* 104, 332-337 (2005).

11. Ashton, T. M., Mckenna, W. G., Kunz-Schughart, L. A. & Higgins, G. S. Oxidative phosphorylation as an emerging target in cancer therapy. *Clinical Cancer Research, clinic cancers* 30, 70-2017 (2018).

12. Dayton P.A. *et al. T*herapeutic gas delivery via microbubbles and liposomes. *Journal of Controlled Release* 209, 139-149 (2015).

13. Benej, M., *et al.*, Papaverine and its derivatives radiosensitize solid tumors by inhibiting mitochondrial metabolism. *Proc Natl Acad Sci USA* 115, 10756-10761 (2018).

14. Rajendran, J. G. & Krohn, K. A. Imaging hypoxia and angiogenesis in tumors. *Radiologic Clinics of North America* 43, 169–187 (2005).

15. Dewhirst, M. W., Cao, Y. & Moeller, B. Cycling hypoxia and free radicals regulate angiogenesis and radiotherapy response. *Nat Rev Cancer* 8, 425–437 (2008).

16. Matsumoto, S., Yasui, H., Mitchell, J. B. & Krishna, M. C. Imaging Cycling Tumor Hypoxia. *Cancer Res* 70, 10019–10023 (2010).

17. Rickard, A. G., Palmer, G. M. & Dewhirst, M. W. Clinical and Pre-clinical Methods for Quantifying Tumor Hypoxia. *Hypoxia and Cancer Metastasis* (2019).

18. Lee, C. T., Boss, M. K. & Dewhirst, M. W. Imaging tumor hypoxia to advance radiation oncology. *Antioxidants & Redox Signaling* 21, 313-337 (2014).

19. Semenza, & Gregg, L. Targeting hif-1 for cancer therapy. *Nature Reviews Cancer* 3, 721-732 (2003).

20. Robert Grimes, D. & Partridge, M. A mechanistic investigation of the oxygen fixation hypothesis and oxygen enhancement ratio. *Biomedical Physics & Engineering Express* 1, 045209 (2015).

21. Freyer, J. P., Jarrett, K., Carpenter, S. & Raju, M. R. Oxygen enhancement ratio as a function of dose and cell cycle phase for radiation-resistant and sensitive Cho cells. *Radiation Research* 127, 297-307 (1991).

22. Fyles, A. W. *et al.* Oxygenation predicts radiation response and survival in patients with cervix cancer. *Radiotherapy and Oncology* 48, 149-156 (1998).

23. Harrison, Louis B. *et al.* Impact of tumor hypoxia and anemia on radiation therapy outcomes. *The oncologist* 7.6: 492-508 (2002).

24. Vaupel, P. & Mayer, A. Hypoxia in cancer: significance and impact on clinical outcome. *Cancer and Metastasis Reviews* 26, 225-239 (2007).

25. Dorn, C. R. Epidemiology of canine and feline tumors. *Journal of the American Animal Hospital Association* 12, 307-312 (1976).

26. Ren, W. *et al.* Combined vascular endothelial growth factor receptor/epidermal growth factor receptor blockade with chemotherapy for treatment of local, uterine, and metastatic soft tissue sarcoma. *Clinical Cancer Research* 14, 5466-5475 (2008).

27. Vaupel, P. & Mayer, A. Hypoxia in cancer: significance and impact on clinical outcome. *Cancer and Metastasis Reviews* 26, 225-239 (2007).

28. Matthews, N. E., Adams, M. A., Maxwell, L. R., Gofton, T. E. & Graham, C. H. Nitric oxide-mediated regulation of chemosensitivity in cancer cells. *Journal of the National Cancer Institute* 93, 1879-1885 (2001).

29. Nordsmark, M. *et al.* Prognostic value of tumor oxygenation in 397 head and neck tumors after primary radiation therapy. An international multi-center study. *Radiotherapy and Oncology* 77, 18-24 (2005).

30. Sun, X., Niu, G., Chan, N., Shen, B., & Chen, X. Tumor hypoxia imaging. *Molecular Imaging and Biology* 13, 399-410 (2011).

31. Lee, C. T., Boss, M. K. & Dewhirst, M. W. Imaging tumor hypoxia to advance radiation oncology. *Antioxidants & redox signaling* 21, 313-337 (2014)

32. Young, R. J., & Andreas Möller. Immunohistochemical detection of tumour hypoxia. *Methods in molecular biology (Clifton, N.J.)* 611, 151-159 (2010).

33. Roussakis, E., Li, Z., Nichols, A. J. & Evans, C. L. Oxygen-sensing methods in biomedicine from the macroscale to the microscale. *Angewandte Chemie International Edition* 54, 8340-8362(2015).

34. Pogue, B. W., & Patterson, M. S. Review of tissue simulating phantoms for optical spectroscopy, imaging and dosimetry. *Journal of Biomedical Optics* 11, 041102 (2006).

35. Madsen, & Steen, J. Optical methods and instrumentation in brain imaging and therapy. *Springer* 2, 23-56 (2013).

36. Nakamura, K., Yamashita, K., Itoh, Y., Yoshino, K., Nozawa, S. & Kasukawa, H. Comparative studies of polyethylene glycol-modified liposomes prepared using different peg-modification methods. *Biochimica et Biophysica Acta* 1818, 2801--2807 (2012).

37. Abou-Saleh, R. H., Swain, M., Evans, S. D. & Thomson, N. H. Poly (ethylene glycol) lipid-shelled microbubbles: abundance, stability, and mechanical properties. *Langmuir* 30, 5557-5563 (2014).

38. Harris, J. M. & Chess, R. B. Effect of pegylation on pharmaceuticals. *Nature Reviews Drug Discovery* 2, 214-221 (2003).

39. Torchilin, & Vladimir, P. Recent advances with liposomes as pharmaceutical carriers. *Nature Reviews Drug Discovery* 4, 145-160 (2005).

40. Sorg, B. S., Moeller, B. J., Cao, Y. & Dewhirst, M. W. Evidence of arteriovenous anastomoses in tumor microvasculature from optical measurements of hemoglobin saturation. *Cancer Research* 65 (2005).

41. Ueda, S., Saeki, T., Takeuchi, H., Shigekawa, T. & Osaki, A. *In vivo* imaging of eribulin-induced reoxygenation in advanced breast cancer patients: a comparison to bevacizumab. *British Journal of Cancer* 114, 1212-1218 (2016).

42. Diaz, P. M. *et al.* Quantitative diffuse reflectance spectroscopy of short-term changes in tumor oxygenation after radiation in a matched model of radiation resistance. *Bio Med. Opt. Express* 9, 3794–3804 (2018).

43. Rojas, A. Radiosensitization with normobaric oxygen and carbogen. *Radiotherapy and Oncology* 20, 65-70 (1991).

44. Dewhirst, M. W., Tso, C. Y., Oliver, R., Gustafson, C. S., Secomb, T. W. & Gross, J. F. Morphologic and hemodynamic comparison of tumor and healing normal tissue microvasculature. *International Journal of Radiation Oncology Biology Physics* 17, 91-99 (1989).

45. Breider, M. A., Ulloa, H. M., Pegg, D. G. & Gough, A. W. Nitro-imidazole radiosensitizer-induced toxicity in cynomolgus monkeys. *Toxicologic Pathology* 26, 651-656 (1998).

46. Papadopoulou, V., Fix S.M., Velds H., Kasoji S.K., Rivera J.N., Borden M.A., Chang S. & Dayton P.A. Oxygen microbubbles to relieve tumor hypoxia *in vivo*, 91st ACS Colloid & Surface Science Symposium. *The City College of New York* (2017).

47. Feshitan J.A., Legband N.D., Borden M.A. & Terry B.S., Systemic oxygen delivery by peritoneal perfusion of oxygen microbubbles. *Biomaterials* 35, 2600-2606 (2014).

48. Kwan J.J., Kaya M., Borden M.A., Dayton P.A., Theranostic oxygen delivery using ultrasound and microbubbles. *Theranostics* 2, 1174-1184 (2012).

49. Hu, F. *et al.* Oxygen and Perfusion Kinetics in Response to Fractionated Radiation Therapy in FaDu Head and Neck Cancer Xenografts Are Related to Treatment Outcome. *International Journal of Radiation Oncology Biology Physics* 96, 462–469 (2016).

50. Fix, S. M. *et al.* Oxygen microbubbles improve radiotherapy tumor control in a rat fibrosarcoma model – a preliminary study. *PLOS ONE* 13, 195-667(2018).

51. Brand, M. & Nicholls, D. Assessing mitochondrial dysfunction in cells. *Biochemical Journal* 437, 575.1-575 (2011).

52. Birsoy, K., Wang, T., Chen, W., Freinkman, E., Abu-Remaileh, M. & Sabatini, D. An essential role of the mitochondrial electron transport chain in cell proliferation is to enable aspartate synthesis. *Cell* 162, 540-551 (2015).

53. Sullivan, L., Gui, D., Hosios, A., Bush, L., Freinkman, E. & Vander, H. M. Supporting aspartate biosynthesis is an essential function of respiration in proliferating cells. *Cell* 162, 552-563 (2015).

54. Calabrese, C., Iommarini, L. & Ivana Kurelac Respiratory complex I is essential to induce a warburg profile in mitochondria-defective tumor cells. *Cancer and Metabolism* 1, 11 (2013).

55. Selak M.A. et al. Succinate links TCA cycle dysfunction to oncogenesis by inhibiting HIF-alpha prolyl hydroxylase. *Cancer Cell* 7, 77–85 (2005).

56. Gasparre, G., Porcelli, A. M., Lenaz, G. & Romeo, G. Relevance of mitochondrial genetics and metabolism in cancer development. *Cold Spring Harbor Perspectives in Biology* 5, 11-41 (2013).

57. Ashton, T. M., Mckenna, W. G., Kunz-Schughart, L. A. & Higgins, G. S. Oxidative phosphorylation as an emerging target in cancer therapy. *Clinical Cancer Research, clincanres* 3070, 2017 (2018).

58. Sharma, L. K., Fang, H., Liu, J., Vartak, R., Deng, J. & Bai, Y. Mitochondrial respiratory complex I dysfunction promotes tumorigenesis through ROS alteration and AKT activation. *Human Molecular Genetics* 20, 4605-4616 (2011).

59. Luisa *et al.* Complex I impairment in mitochondrial diseases and cancer: parallel roads leading to different outcome. *The International Journal of Biochemistry & Cell Biology* (2013).

60. Alberto Cruz-Bermúdez, Vallejo, C. G., Vicente-Blanco, R. J., María Esther Gallardo & Garesse, R. Enhanced tumorigenicity by mitochondrial DNA mild mutations. *Oncotarget* 6, 13628-13643 (2015).

61. Li, B. *et al.* Inhibition of complex I regulates the mitochondrial permeability transition through a phosphate-sensitive inhibitory site masked by cyclophilin D. *Bioenergetics*, 1817, 1628-1634 (2012).

62. Sharma, L. K., Fang, H., Liu, J., Vartak, R., Deng, J. & Bai, Y. Mitochondrial respiratory complex I dysfunction promotes tumorigenesis through ROS alteration and AKT activation. *Human Molecular Genetics* 20, 4605-4616 (2011).

63. Kruuv, J. A., Inch, W. R. & Mccredie, J. A. Blood flow and oxygenation of tumors in mice. I. effects of breathing gases containing carbon dioxide at atmospheric pressure. *Cancer* 20, 51-59 (1967).

64. Secomb, T. W., Hsu, R. & Dewhirst, M. W. Synergistic effects of hyperoxic gas breathing and reduced oxygen consumption on tumor oxygenation: a theoretical model. *International Journal of Radiation Oncology Biology Physics* 59, 572-578 (2004).

65. Eisenbrey, J.R. *et al.* Sensitization of hypoxic tumors to radiation therapy using ultrasound-sensitive oxygen microbubbles. *International Journal of Radiation Oncology, Biology, Physics* 101, 88-96 (2018).

66. Dawson, R. B. J., Kocholaty, W. F. & Gray, J. L. Hemoglobin function and 2,3-dpg levels of blood stored at 4C in ACD and CPD: pH effect. *Transfusion* 10, 299-304 (1970).

67. Yasui, H. *et al.* Low-field magnetic resonance imaging to visualize chronic and cycling hypoxia in tumor-bearing mice. *Cancer Research* 70, 6427-6436 (2010).

68. Johnson, J. *et al.* Relationships between drug activity in NCI preclinical *in vitro* and *in vivo* models and early clinical trials. *Br. J. Cancer* 84, 1424-1431(2001)

69. Gort, E. H. et al. The twist1 oncogene is a direct target of hypoxia-inducible factor-2α. *ONCOGEN* 27, 1501-1510 (2007).

70. Kaidi, A., Williams, A. C. & Paraskeva, C. Interaction between β-catenin and HIF-1 promotes cellular adaptation to hypoxia. *Nature Cell Biology* 9, 210-217 (2007).

71. Muhammad, K. et al. Oxygen-carrying micro/nanobubbles: composition, synthesis techniques and potential prospects in photo-triggered theranostics. *Molecules* 23, 2210 (2018).